

1 **Palaeoclimatic oscillations in the Pliensbachian (Early Jurassic) of the Asturian Basin**
2 **(Northern Spain).**

3 J.J. Gómez¹, M.J. Comas-Rengifo² and A. Goy³

4

5 ¹ Departamento de Estratigrafía, Facultad de Ciencias Geológicas (UCM) and Instituto de
6 Geociencias (CSIC-UCM). 28040 Madrid. Spain

7 ² Departamento de Paleontología, Facultad de Ciencias Geológicas (UCM). 28040
8 Madrid. Spain

9 ³ Departamento de Paleontología, Facultad de Ciencias Geológicas (UCM) and Instituto
10 de Geociencias (CSIC-UCM). 28040 Madrid. Spain

11

12 *Correspondence to:* igomez@ucm.es

13

14 **Abstract.**

15 One of the main controversial **themes** in palaeoclimatology involves elucidating
16 whether climate during the Jurassic was warmer than the present day and if it was the
17 same over Pangea, with no major latitudinal gradients. There have been abundant
18 evidences of oscillations in seawater temperature throughout the Jurassic. The
19 Pliensbachian (Early Jurassic) constitutes a distinctive time interval for which several
20 seawater temperature oscillations, including an exceptional cooling event, have been
21 documented. To constrain the timing and magnitude of these climate changes, the
22 Rodiles section of the Asturian Basin (Northern Spain), a well exposed succession of
23 the uppermost Sinemurian, Pliensbachian and Lower Toarcian deposits, has been
24 studied. A total of 562 beds were measured and sampled for ammonites, for
25 biochronostratigraphical purposes, and for belemnites, to determine the
26 palaeoclimatic evolution through stable isotope studies. Comparison of the recorded
27 latest Sinemurian, Pliensbachian and Early Toarcian changes in seawater
28 palaeotemperature with other European sections allows characterization of several
29 climatic changes that are likely of a global extent. A warming interval partly coinciding
30 with a $\delta^{13}\text{C}_{\text{bel}}$ negative excursion was recorded at the Late Sinemurian. After a
31 “normal” temperature interval, a new warming interval containing a short-lived
32 positive $\delta^{13}\text{C}_{\text{bel}}$ peak, developed during the Early–Late Pliensbachian transition. The
33 Late Pliensbachian represents an outstanding cooling interval containing a $\delta^{13}\text{C}_{\text{bel}}$
34 positive excursion interrupted by a small negative $\delta^{13}\text{C}_{\text{bel}}$ peak. Finally, the Early
35 Toarcian represented an exceptional warming period, which has been pointed as being
36 the main responsible for the prominent Early Toarcian mass extinction.

37 **Introduction**

38 The idea of an equable Jurassic greenhouse climate, 5–10° C warmer than present day,
39 with no ice caps and presenting a low pole-equator temperature gradient, has been

40 proposed in several studies (i.e. Hallam, 1975, 1993; Chandler et al., 1992; Frakes et
41 al., 1992; Rees et al., 1999). Nevertheless, this hypothesis has been challenged by
42 numerous palaeoclimatic studies, mainly based on palaeotemperature calculations
43 making use of the oxygen isotope data from belemnite and brachiopod calcite as a
44 proxy.

45 Especially relevant are the latest Pliensbachian–Early Toarcian climate changes, which
46 have been documented in many sections from Western Europe (i. e. Sælen et al., 1996;
47 McArthur et al., 2000; Röhl et al., 2001; Schmidt-Röhl et al., 2002; Bailey et al., 2003;
48 Jenkyns, 2003; Rosales et al., 2004; Gómez et al., 2008; Metodiev and Koleva-Rekalova,
49 2008; Suan et al., 2008, 2010; Dera et al., 2009, 2010, 2011; Gómez and Arias, 2010;
50 García Joral et al., 2011; Gómez and Goy, 2011; Fraguas et al., 2012), as well as in
51 Northern Siberia and in the Artic Region (Zakharov et al., 2006; Nikitenko, 2008; Suan
52 et al., 2011). The close correlation between the severe Late Pliensbachian Cooling and
53 the Early Toarcian Warming events, and the major Early Toarcian mass extinction
54 indicates that warming was one of the main causes of this faunal turnover (Kemp et
55 al., 2005; Gómez et al., 2008; Gómez and Arias, 2010; García Joral et al., 2011; Gómez
56 and Goy, 2011; Fraguas et al., 2012; Clémence, 2014; Clémence et al., 2015; Baeza-
57 Carratalá et al., 2015).

58 Nevertheless, with the exception of several sections (Rosales et al., 2004; Korte and
59 Hesselbo, 2011; Suan et al., 2008, 2010), few data have been published on the evolution
60 of seawater palaeotemperatures during the latest Sinemurian and the Pliensbachian,
61 even some more papers studied the climatic changes of parts of the Late Pliensbachian
62 and Early Toarcian (i.e. McArthur et al., 2000; Hesselbo et al., 2000; Jenkyns et al.,
63 2002; van de Schootbrugge et al., 2010; Gómez and Goy, 2011; Armendáriz et al.,
64 2012; Harazim et al., 2013).

65 The present paper attempts to provide data on the evolution of seawater
66 palaeotemperatures and on changes in carbon isotopes through the Late Sinemurian,
67 Pliensbachian and Early Toarcian (Early Jurassic) and to constrain the timing of the
68 recorded changes through ammonite-based biochronostratigraphy. The dataset was
69 obtained from the particularly well exposed Rodiles section, located in the Asturias
70 regional autonomy in Northern Spain (Fig. 1). Our results have been correlated with
71 the records obtained in different sections of Europe, showing that these climatic
72 changes, as well as the documented perturbations of the carbon cycle, could be of
73 global, or at least of regional extent at European scale.

74 **2 Materials and methods**

75 In the coastal cliffs located northeast of the Villaviciosa village, in the eastern part of
76 the Asturias regional autonomy (Northern Spain) (Fig. 1), the well exposed Upper
77 Sinemurian, Pliensbachian and Lower Toarcian deposits are represented by a
78 succession of alternating lime mudstone to bioclastic wackestone and marls with
79 interbedded black shales belonging to the Santa Mera Member of the Rodiles
80 Formation (Valenzuela, 1988) (Fig. 2). The uppermost Sinemurian and Pliensbachian
81 deposits were studied in the eastern part of the Rodiles Cape and the uppermost
82 Pliensbachian and Lower Toarcian in the western part of the Rodiles Cape (West
83 Rodiles section of Gómez et al., 2008; Gómez and Goy 2011). Both fragments of the

84 section are referred to here as the Rodiles section (lat. 43°32'22" long. 5°22'22").
85 Palaeogeographical reconstruction based on comprehensive palaeomagnetic data,
86 performed by Osete et al. (2010), locates the Rodiles section studied at a latitude of
87 approximately 32° N for the Hettangian–Sinemurian interval, which is in good
88 agreement with the calculations of Van Hinsbergen et al. (2015) and at a latitude of
89 almost 40° N (the current latitude of Madrid) for the Toarcian–Aalenian interval. The
90 section was deposited in an open marine external platform environment with sporadic
91 intervals of oxygen deficiency.

92 The 110 m thick section studied, comprising 562 beds, was studied bed by bed.
93 Collected ammonites were prepared and studied following the habitual
94 palaeontological methods (Comas-Rengifo, 1985; Phelps, 1985; Howarth, 2002). The
95 biochronostratigraphy obtained enabled characterization of the standard chronozones
96 and subchronozones established by Elmi et al. (1997) and Page (2003), which are used
97 in the present research.

98 A total of 191 analyses of stable isotopes were performed on 163 belemnite calcite
99 samples, in order to obtain the primary Late Sinemurian, Pliensbachian and Early
100 Toarcian seawater stable isotope signal, and hence to determine palaeotemperature
101 changes, as well as the variation pattern of the carbon isotope in the studied time
102 interval. In order to assess possible burial diagenetic alteration of the belemnites,
103 polished samples and thick sections of each belemnite rostrum were prepared. The
104 thick sections were studied under the petrographic and the cathodoluminescence
105 microscope, and only the non-luminescent, diagenetically unaltered portions of the
106 belemnite rostrum, were sampled using a microscope-mounted dental drill. Sampling
107 of the luminescent parts such as the apical line and the outer and inner rostrum wall,
108 fractures, stylolites and borings were avoided. Belemnite calcite was processed in the
109 stable isotope labs of the Michigan University (USA), with a Finnigan MAT 253 triple
110 collector isotope ratio mass spectrometer. The procedure followed in the stable
111 isotope analysis has been described in Gómez and Goy (2011). Isotope ratios are
112 reported in per mil relative to the standard PeeDee belemnite (PDB), presenting a
113 reproducibility better than 0.02 ‰ PDB for $\delta^{13}\text{C}$ and better than 0.06 ‰ PDB for $\delta^{18}\text{O}$.

114 The seawater palaeotemperature recorded in the oxygen isotopes of the belemnite
115 rostra studied have been calculated using the Anderson and Arthur (1983) equation:
116 $T(\text{°C}) = 16.0 - 4.14 (\delta_c - \delta_w) + 0.13 (\delta_c - \delta_w)^2$ where $\delta_c = \delta^{18}\text{O}$ PDB is the composition of the
117 sample, and $\delta_w = \delta^{18}\text{O}$ SMOW the composition of ambient seawater. Following the
118 recommendations of Shackleton and Kennett (1975), the standard value of $\delta_w = -1\text{‰}$
119 was used for palaeotemperature calculations under non-glacial ocean water
120 conditions. If the presence of permanent ice caps in the poles is demonstrated for
121 some of the intervals studied, value of $\delta_w = 0\text{‰}$ would be used and consequently
122 calculated palaeotemperatures would increase in the order of 4°C.

123 To calculate palaeotemperature, it has been assumed that the $\delta^{18}\text{O}$ values, and
124 consequently the resultant curve, essentially reflects changes in environmental
125 parameters (Sælen et al., 1996; Bettencourt and Guerra, 1999; McArthur et al., 2007;
126 Price et al., 2009; Rexfort and Mutterlose, 2009; Benito and Reolid, 2012; Li et al.,
127 2012; Harazim et al., 2013; Ullmann et al., 2014, Ullmann and Korte, 2015), as the
128 sampled non-luminescent biogenic calcite of the studied belemnite rostra precipitated

129 in equilibrium with the seawater. It has also been assumed that the biogenic calcite
130 retains the primary isotopic composition of the seawater and that the belemnite
131 migration, skeletal growth, sampling bias, and vital effects do not constitute the main
132 factors responsible for the variations obtained.

133 **2.1. Reliability of belemnite isotope records**

134 Discussion of the palaeoecology of belemnites, or the validity of the isotopic data
135 obtained from belemnite calcite for the calculation of palaeotemperatures do not fall
136 within the scope of this research, but the use of belemnite calcite as a proxy is
137 generally accepted and widely used as a reliable tool for palaeothermometry in most
138 of the Mesozoic. However, belemnite palaeoecology constitutes a source of conflicts
139 because, due to the fact that these organisms are extinct, there is a complete lack of
140 understanding of fossil belemnite ecology (Rexfort and Mutterlose, 2009). Belemnites
141 lived as active predators within swimming life habitats. Nevertheless, several authors
142 (Anderson et al., 1994; Mitchell, 2005; Wierzbowski and Joachimiski, 2007) have
143 proposed a bottom-dwelling lifestyle on the basis of oxygen isotope thermometry,
144 similar to modern sepiids which show a nektobenthic mode of life. This is contradicted
145 by the occurrence of various belemnite genera in black shales which lack any benthic
146 or nektobenthic organisms due to the existence of anoxic bottom waters (i.e. the
147 Lower Jurassic Posidonienschiefer, see Rexfort and Mutterlose, 2009), a fact that
148 indicates that belemnites presented a nektonic mode of life rather than a nektobenthic
149 (Mutterlose et al., 2010). As Rexfort and Mutterlose (2009) stated, it is unclear
150 whether isotopic data from belemnites reflect a surface or a deeper water signal, and
151 we are unaware whether the belemnites mode of life changed during ontogeny.
152 Similarly, Li et al. (2012) concluded that belemnites were mobile and experienced a
153 range of environmental conditions during growth; furthermore, these authors stated
154 that some belemnite species inhabited environmental niches that remain unchanged,
155 while other species had a more cosmopolitan lifestyle inhabiting wider environments.
156 To complete the scenario, Mutterlose et al. (2010) suggested different lifestyles
157 (nektonic versus nektobenthic) of belemnite genera as indicated by different shaped
158 guards. Short, thick guards could indicate nektobenthic lifestyle, elongated forms fast
159 swimmers, and extremely flattened guards a benthic lifestyle.
160 The study by Ullmann et al. (2014) hypothesises that belemnites (*Passaloteuthis*) of
161 the Lower Toarcian Tenuicostatum Zone had a nektobenthic lifestyle and once became
162 extinct (as many organisms in the Early Toarcian mass extinction) were substituted by
163 belemnites of the genus *Acrocoelites* supposedly with a nektonic lifestyle, which these
164 authors attribute to anoxia.
165 The isotopic studies performed on present-day cuttlefish (*Sepia* sp.), which are
166 assumed to constitute the group most equivalent to belemnites, reveals that all the
167 specimens (through their $\delta^{18}\text{O}$ signal) perfectly reflect the temperature-characteristics
168 of their habitat (Rexfort and Mutterlose, 2009). Also the studies of Bettencourt and
169 Guerra (1999), performed in cuttlebone of *Sepia officinalis*, conclude that the $\delta^{18}\text{O}$
170 obtained temperature agreed with changes in seawater temperature, thus supporting
171 the use of belemnites as excellent tools for calculation of palaeotemperatures.
172 It seems that at least some belemnites could swim through the water column,
173 reflecting average temperature and not necessarily only bottom or surface water
174 temperatures. In any case, rather than single specific values, in the present paper

175 comparisons of average temperatures to define the different episodes of temperature
176 changes are used.

177 **3 Results**

178 Ammonite taxa distribution and profiles of the $\delta^{18}\text{O}_{\text{bel}}$, $\delta^{13}\text{C}_{\text{bel}}$ and $\delta^{13}\text{C}_{\text{bulk}}$ values
179 obtained from belemnite calcite have been plotted against the 562 measured beds of
180 the Rodiles section (Fig. 3).

181 **3.1 Lithology**

182 The Upper Sinemurian, Pliensbachian and Lower Toarcian deposits of the Rodiles
183 section comprise couplets of bioclastic lime mudstone to wackestone limestone and
184 marls. These limestones occasionally contain bioclastic packstone facies concentrated
185 in rills. Limestones, generally recrystallized to microsparite, are commonly well
186 stratified in beds whose continuity can be followed at the outcrop scale, as well as in
187 outcrops several kilometres apart. However, nodular limestone layers, discontinuous
188 at the outcrop scale, are also present. The base of some carbonates can be slightly
189 erosive, and they are commonly bioturbated, to reach the homogenization stage.
190 Ichnofossils, especially *Thalassinoides*, *Chondrites* and *Phymatoderma*, are also
191 present. Marls, with CaCO_3 content generally lower than 20% (Bádenas et al., 2009,
192 2012), are frequently grey coloured, occasionally light grey due to the higher
193 proportion of carbonates, with interbedded black intervals. Locally brown coloured
194 sediments are present, more often in the Upper Sinemurian.

195 **3.2 Biochronostratigraphy**

196 The ammonite-based biochronostratigraphy of these deposits in Asturias was
197 performed by Suárez-Vega (1974), and the uppermost Pliensbachian and Toarcian
198 ammonites by Gómez et al. (2008), and by Goy et al. (2010 a, b). Preliminary
199 biochronostratigraphy of the Late Sinemurian and the Pliensbachian in some sections
200 of the Asturian Basin has been reported by Comas-Rengifo and Goy (2010), and herein
201 we summarise the result of over ten years of bed by bed sampling of ammonites in the
202 Rodiles section, which provided a precise time constraint for the climatic events
203 described in this work.

204 The ammonites collected enabled recognition of all the standard Late Sinemurian,
205 Pliensbachian and Early Toarcian chronozones and subchronozones defined by Elmi et
206 al. (1997) and Page (2003) for Europe. The section is generally expanded and
207 ammonites are sufficiently common to constrain the boundaries of the
208 biochronostratigraphical units. Exceptions are the *Taylori–Polymorphus*
209 subchronozones that could not be separated, and the *Capricornus–Figulinum*
210 subchronozones of the *Davoei* Chronozone, partly due to the relatively condensed
211 character of this Chronozone. Most of the recorded species belong to the NW Europe
212 province but some representatives of the Tethysian Realm are also present.

213 **3.3 Belemnite preservation**

214 Belemnites in the Rodiles section generally show an excellent degree of preservation
215 (Fig. 4) and none of the prepared samples were rejected, as only the non-luminescent

216 parts of the belemnite rostrum not affected by diagenesis were selected. It has been
217 assumed that the biogenic calcite retains the primary isotopic composition of the
218 seawater and that the belemnite migration, skeletal growth, sampling bias, and vital
219 effects are not the main factors responsible for the variations obtained.

220 The cross-plot of the $\delta^{18}\text{O}$ against the $\delta^{13}\text{C}$ values (Fig. 5) reveals a cluster-type
221 distribution, showing a negative correlation coefficient (-0.2) and very low covariance
222 ($R^2=0.04$), supporting the lack of diagenetic overprints in the diagenetically screened
223 belemnite calcite analyzed.

224 3.4 Carbon isotopes

225 The carbon isotopes curve reflects several oscillations **throughout** the section **studied**
226 (**Fig. 5**). A positive $\delta^{13}\text{C}_{\text{bel}}$ shift, showing average values of $1.6\text{\textperthousand}$ is recorded **from** the
227 Late Sinemurian Densinodulum to part of the Macdonnelli subchronozones (**from**
228 **meter 0 to 21 in Fig. 3**). From the **latest** Sinemurian Aplanatum Subchronozone
229 (**Raricostatum Chronozone**) up to the **Early** Pliensbachian Valdani Subchronozone of
230 the Ibex Chronozone, average $\delta^{13}\text{C}_{\text{bel}}$ values are $-0.1\text{\textperthousand}$, delineating **an approximately**
231 $1-1.5\text{\textperthousand}$ relatively well marked negative excursion (**from meter 21 to 73 in Fig. 3**). In the
232 **late** Ibex and **in** the Davoei chronozones, the $\delta^{13}\text{C}_{\text{bel}}$ curve records background values
233 of **around** 1\textperthousand , with a positive **excursion** at the **latest** Ibex Chronozone and the **earliest**
234 **Davoei Chronozone** (**from meter 58 to 71 in Fig. 3**).

235 At the **Late** Pliensbachian the $\delta^{13}\text{C}_{\text{bel}}$ values tend to outline a slightly positive excursion
236 (**from meter 73 to 98 in Fig. 3**), interrupted by a small negative peak in the **latest**
237 **Spinatum Chronozone** (**from meter 98 to 103 in Fig. 3**). The **Early** Toarcian curve
238 reflects the presence of a positive $\delta^{13}\text{C}_{\text{bel}}$ trend which develops above the
239 stratigraphical levels **represented herein**, up to the Middle Toarcian Bifrons
240 Chronozone (Gómez et al., 2008) **and a negative excursion recorded in bulk carbonates**
241 **samples**.

242 3.5 Oxygen isotopes

243 The $\delta^{18}\text{O}_{\text{bel}}$ values show the presence of several excursions **throughout** the **Late**
244 **Sinemurian** to the **Early** Toarcian (**Fig. 3**). **From** the **Late** Sinemurian to the **earliest**
245 **Pliensbachian** interval, a negative excursion **of around** 1\textperthousand , showing values generally
246 below $-1\text{\textperthousand}$ with peak values up to $-3\text{\textperthousand}$ has been recorded in Sinemurian samples
247 located immediately below the stratigraphic column represented in Fig. 3. In most of
248 the **Early** Pliensbachian Jamesoni and the **earliest part** of the Ibex chronozones, $\delta^{18}\text{O}_{\text{bel}}$
249 values are quite stable, around $-1\text{\textperthousand}$, but another negative excursion **of approximately**
250 $1-1.5\text{\textperthousand}$, with peak values up to $-1.9\text{\textperthousand}$, develops along most of the **Early**
251 **Pliensbachian** Ibex and Davoei chronozones, extending up to the base of the **Late**
252 **Pliensbachian** Margaritatus Chronozone. Most of the **Late** Pliensbachian and the
253 **earliest** Toarcian are characterized by the presence of a **significant** change. **In this**
254 **interval** a positive excursion **in the order of** $1.5\text{\textperthousand}$ $\delta^{18}\text{O}_{\text{bel}}$, with frequent values **of**
255 **around** 0\textperthousand , and positive values up to $0.7\text{\textperthousand}$, were assayed. The oxygen isotopes
256 recorded a new change **in** its tendency in the **Early** Toarcian, where a prominent $\delta^{18}\text{O}_{\text{bel}}$
257 **negative excursion**, about $1.5-2\text{\textperthousand}$ with values up to $-3\text{\textperthousand}$, has been verified.

258 4 Discussion

259 The isotope curves obtained in the Upper Sinemurian, Pliensbachian and Lower
260 Toarcian section of the Asturian Basin has been correlated with other successions of a
261 similar age, in order to evaluate whether the environmental features recorded present
262 a local or possible global extent. In order to correlate a more homogeneous dataset,
263 we only employed the isotopic results obtained by other authors from belemnite
264 calcite and exceptionally from brachiopod calcite, have been used to correlate the
265 stable isotopic data.

266 **4.1. Updated stratigraphy**

267 The detailed biostratigraphical analysis, based on the succession of the Pliensbachian
268 ammonoids assemblages allowed construction of a scale of reference that has
269 facilitated the location of the different palaeoclimatic events recognized in the present
270 research.

271 The five biochronozones of the standard scale constituting the Pliensbachian of the
272 Subboreal/NW Europe Province (Dommergues et al., 1997; Page, 2003) have been
273 recognized in the Rodiles section. For the first time, these biochronozones have been
274 subdivided into 14 subchronozones whose boundaries have been corrected in many
275 cases respect to previous studies. In most cases these boundaries have now been
276 established with a low margin of uncertainty.

277 With regard to previous research (Suárez-Vega, 1974; Comas-Rengifo and Goy, 2010)
278 the Taylori and Brevispina subchronozones of the Early Pliensbachian have been
279 characterized in this study for the first time, and the boundary between the Valdani
280 and the Luridum subchronozones, usually difficult to distinguish in the Asturian Basin,
281 has been clearly recognized. In the Late Pliensbachian, where the record of Amaltheidae
282 is quite complete, the subchronozone Apyrenum of the Spinatum Chronozone has
283 been characterized and the boundary between the Subnodosus and Gibbosus
284 subchronozones has been precisely established.

285 **4.2. Carbon isotope curve**

286 The $\delta^{13}\text{C}_{\text{bel}}$ carbon isotope excursions (CIEs) found in the Asturian Basin, can be
287 followed in other sections across Western Europe (Fig. 6). The Late Sinemurian positive
288 CIE was also recorded in the Cleveland Basin of the UK by Korte and Hesselbo (2011)
289 and in the $\delta^{13}\text{C}_{\text{org}}$ data of the Wessex Basin of southern UK by Jenkyns and Weedon
290 (2013).

291 The Early Pliensbachian $\delta^{13}\text{C}_{\text{bel}}$ negative excursion extending from the Raricostatum
292 Chronozone of the latest Sinemurian to the Early Pliensbachian Jamesoni and part of
293 the Ibex chronozones (Fig. 6), correlates with the lower part of the $\delta^{13}\text{C}_{\text{bel}}$ negative
294 excursion reported by Armendáriz et al. (2012) in another section of the Asturian
295 Basin. Similarly, the $\delta^{13}\text{C}_{\text{bel}}$ curve obtained by Quesada et al. (2005) in the neighbouring
296 Basque–Cantabrian Basin shows the presence of a negative CIE in a similar
297 stratigraphical position. In the Cleveland Basin in the UK, the studies on the
298 Sinemurian–Pliensbachian deposits conducted by Hesselbo et al. (2000), Jenkyns et al.
299 (2002) and Korte and Hesselbo (2011) reflect the presence of this Early Pliensbachian
300 $\delta^{13}\text{C}_{\text{bel}}$ decrease in values. In the Peniche section of the Lusitanian Basin of Portugal,
301 this negative CIE was also recorded by Suan et al. (2010) in brachiopod calcite, and in

302 bulk carbonates in Italy (Woodfine et al., 2008; Francheschi et al., 2014). The
303 magnitude of approximately 1.5–2‰ of this negative excursion appears to be quite
304 consistent across the different European localities.

305 Korte and Hesselbo (2011) pointed out that the Early Pliensbachian $\delta^{13}\text{C}$ negative
306 excursion seems to be global in character, resulting from the injection of isotopically
307 light carbon from some remote source, such as methane from clathrates, wetlands, or
308 thermal decomposition, thermal metamorphism or decomposition of older organic-
309 rich deposits. However, none of these possibilities have as yet been documented.

310 Higher in the section, the $\delta^{13}\text{C}$ values are relatively uniform, except for a thin interval,
311 around the Early Pliensbachian Ibex–Davoei zonal boundary, where a small positive
312 excursion (the Ibex–Davoei positive excursion, previously mentioned by Rosales et al.,
313 2001 and by Jenkyns et al., 2002) can be observed in most of the $\delta^{13}\text{C}$ curves
314 summarized in Fig. 6, as well as in the carbonates of the Portuguese Lusitanian Basin
315 (Silva et al., 2011).

316 The next CIE involves a positive excursion of around 1.5–2‰, well recorded in all the
317 correlated Upper Pliensbachian sections (the Late Pliensbachian positive excursion in
318 Fig. 6) and in bulk carbonates of the Lusitanian Basin (Silva et al., 2011; Silva and
319 Duarte, 2015) and in the Apennines of Central Italy (Moretini et al., 2002). This CIE
320 also partly coincides with the $\delta^{13}\text{C}_{\text{org}}$ reported by Caruthers et al. (2014) in Western
321 North America. Around the Pliensbachian–Toarcian boundary, a negative $\delta^{13}\text{C}$ peak is
322 once again recorded (Fig. 6). This narrow excursion was described by Hesselbo et al.
323 (2007) in bulk rock samples in Portugal, and tested by Suan et al. (2010) in the same
324 basin and extended to the Yorkshire (UK) by Littler et al. (2010) and by Korte and
325 Hesselbo (2011). If this perturbation of the carbon cycle is global, as Korte and
326 Hesselbo (2011) pointed out, it could correspond with the negative $\delta^{13}\text{C}$ peak recorded
327 in the upper part of the Spinatum Chronozone in the Asturian Basin (present paper);
328 with the negative $\delta^{13}\text{C}$ peak reported by Quesada et al. (2005) in the same
329 stratigraphical position in the Basque–Cantabrian Basin, and with the $\delta^{13}\text{C}$ negative
330 peak reported by van de Schootbrugge et al. (2010) and Harazim et al. (2013) in the
331 French Grand Causses Basin.

332 Finally, the Early Toarcian is characterized by a prominent $\delta^{13}\text{C}$ positive excursion that
333 has been detected in all the sections considered herein, as well as in some South
334 American (Al-Suwaidei et al., 2010) and Northern African (Bodin et al., 2010) sections.
335 This positive CIE is interrupted by a negative excursion of approximately 1‰ $\delta^{13}\text{C}_{\text{bulk}}$
336 located around the Tenuicostatum–Serpentinum zonal boundary.

337 The origin of the positive excursion has been interpreted by some authors as the
338 response of water masses to excess and rapid burial of large amounts of organic
339 carbon rich in ^{12}C , which led to enrichment in ^{13}C of the sediments (Jenkyns and
340 Clayton, 1997; Schouten et al., 2000). Other authors ascribe the origin of this positive
341 excursion to the removal from the oceans of large amounts of isotopically light carbon
342 as organic matter into black shales or methane hydrates, resulting from ebullition of
343 isotopically heavy CO_2 , generated by methanogenesis of organic-rich sediments
344 (McArthur et al., 2000).

345 Although $\delta^{13}\text{C}$ positive excursions are difficult to account for (Payne and Kump, 2007),
346 it seems that this positive CIE cannot necessarily be the consequence of the
347 widespread preservation of organic-rich facies under anoxic waters, as no anoxic facies
348 are present in the Spanish Lower Toarcian sections (Gómez and Goy, 2011). Modelling
349 of the CIEs performed by Kump and Arthur (1999) shows that $\delta^{13}\text{C}$ positive excursions
350 can also be due to an increase in the rate of phosphate or phosphate and inorganic
351 carbon delivery to the ocean, and that large positive excursions in the isotopic
352 composition of the ocean can also result from an increase in the proportion of
353 carbonate weathering relative to organic carbon and silicate weathering. Other
354 authors argue that an increase of $\delta^{13}\text{C}$ in bulk organic carbon may reflect a massive
355 expansion of marine archaea bacteria that do not isotopically discriminate in the type
356 of carbon they use, giving rise to positive $\delta^{13}\text{C}$ shifts (Kidder and Worsley, 2010).

357 The origin of the Early Toarcian $\delta^{13}\text{C}$ negative excursion has been explained by several
358 papers as resulting from the massive release of large amounts of isotopically light CH_4
359 from the thermal dissociation of gas hydrates. Hesselbo et al. (2000, 2007), Cohen et
360 al. (2004) and Kemp et al. (2005), associated it with the massive release of gas
361 methane linked with the intrusion of the Karoo-Ferrar large igneous province onto
362 coalfields, as proposed by McElwain et al. (2005) or with the contact metamorphism by
363 dykes and sills related to the Karoo-Ferrar igneous activity into organic-rich sediments
364 (Svensen et al., 2007).

365 Martinez and Dera (2015) proposed the presence of fluctuations in the carbon cycle
366 during the Jurassic and Early Cretaceous, resulting from a cyclicity of ~9 My linked to a
367 great eccentricity cycle, amplified by cumulative sequestration of organic matter.
368 Nevertheless, this ~9 My cycle has not been evidenced in the Pliensbachian deposits of
369 several parts of the World (Ikeda and Tada, 2013, 2014) and cannot be evidenced in
370 the Pliensbachian deposits of the Asturian Basin either. The disruption of this cyclicity
371 recorded during the Pliensbachian could be linked to chaotic behaviour in the solar
372 system (Martinez and Dera, 2015) possibly due to the chaotic transition in the
373 Earth–Mars resonance (Ikeda and Tada, 2013). Data from Japan suggests that this
374 disruption, which developed from the Hettangian to the Pliensbachian (Ikeda and
375 Tada, 2013, 2014) was possibly linked to the massive injection of CO_2 from the
376 eruptions of the Central Atlantic Magmatic Province to the Karoo-Ferrar eruptions
377 (Prokoph et al. 2013) which destabilized the carbon fluxes, reducing or dephasing the
378 orbital imprint in the $\delta^{13}\text{C}$ over millions of years (Martinez and Dera, 2015).

379 **4.3. Oxygen isotope curves and seawater palaeotemperature oscillations**

380 Seawater palaeotemperature calculation from the $\delta^{18}\text{O}$ values obtained reveals the
381 occurrence of several isotopic events corresponding to relevant climatic oscillations
382 across the latest Sinemurian, the Pliensbachian and the Early Toarcian (Fig. 7). Some of
383 these climatic changes could be of global extent. In terms of seawater
384 palaeotemperature, five intervals can be distinguished. The earliest interval of these
385 corresponds to a warming period developed from the Late Sinemurian up to the
386 earliest Pliensbachian. Most of the Early Pliensbachian is represented by a period of
387 “normal” temperature, close to the average palaeotemperatures of the interval
388 studied. A new warming period is recorded in the Early–Late Pliensbachian transition,
389 and the Late Pliensbachian is represented by an important cooling interval. Finally the

390 Early Toarcian coincides with a severe (super)warming interval, linked to the important
391 Early Toarcian mass extinction (Gómez and Arias, 2010; García Joral et al., 2011;
392 Gómez and Goy, 2011; Fraguas et al., 2012; Clémence, 2014; Clémence et al., 2015;
393 Baeza-Carratalá et al., 2015). The average palaeotemperature of the latest Sinemurian,
394 Pliensbachian (palaeolatitude of 32°N) and Early Toarcian (palaeolatitude of 40°N),
395 calculated from the $\delta^{18}\text{O}$ values obtained from belemnite calcite in the present study,
396 is 15.6°C. As mentioned above, some belemnites could swim through the water
397 column, and the palaeotemperatures calculated do not necessarily correspond only
398 with the temperatures of the bottom or surface waters, but also the average
399 temperature.

400 **4.3.1. The Late Sinemurian Warming**

401 The earliest isotopic event is a $\delta^{18}\text{O}$ negative excursion that develops from the Late
402 Sinemurian Raricostatum Chronozone, up to the earliest Pliensbachian Jamesoni
403 Chronozone. Average palaeotemperatures calculated from the $\delta^{18}\text{O}$ belemnite samples
404 collected below the part of the Late Sinemurian Raricostatum Chronozone represented
405 in figure 7 were 19.6°C. This temperature increases to 21.5°C in the lower part of the
406 Raricostatum Chronozone (Densinodulum Subchronozone), and progressively
407 decreases throughout the latest Sinemurian and earliest Pliensbachian. In the
408 Raricostatum Subchronozone, the average temperature calculated is 18.7°C; in the
409 Macdonnelli Subchronozone average temperature is 17.5°C and average values of
410 16.7°C, closer to the average temperatures of the studied interval, are not reached
411 until the latest Sinemurian Aplanatum Subchronozone and the earliest Pliensbachian
412 Taylori–Polymorphus subchronozones. All these values delineate a warming interval
413 mainly developed in the Late Sinemurian (Figs. 7, 8) in which the general trend involves
414 a decrease in palaeotemperature from the Late Sinemurian to the earliest
415 Pliensbachian.

416 The Late Sinemurian Warming interval is also recorded in the Cleveland Basin in the UK
417 (Hesselbo et al., 2000; Korte and Hesselbo, 2011). The belemnite-based $\delta^{18}\text{O}$ values
418 obtained by these authors are in the order of $-1\text{\textperthousand}$ to $-3\text{\textperthousand}$, with peak values lower
419 than $-4\text{\textperthousand}$. This represents a range of palaeotemperatures normally between 16 and
420 24°C with peak values of up to 29°C, which are not compatible with a cooling interval,
421 but rather with a period of warming.

422 The Late Sinemurian warming coincides only partly with the Early Pliensbachian $\delta^{13}\text{C}$
423 negative excursion, located near the stage boundary (Fig. 6). Consequently, this
424 warming cannot be fully interpreted as the consequence methane release from
425 clathrates, wetlands or decomposition of older organic-rich sediments, as interpreted
426 by Korte and Hesselbo (2011) because only a small portion of both excursions are
427 coincident.

428 **4.3.2. The “normal” temperature in the Early Pliensbachian Jamesoni Chronozone
429 interval**

430 Following the Late Sinemurian Warming, $\delta^{18}\text{O}$ values are around $-1\text{\textperthousand}$ reflecting
431 average palaeotemperatures of approximately 16°C (Fig. 7). This Early Pliensbachian
432 interval of “normal” (average) temperature develops in most of the Jamesoni

433 Chronozone and in the base of the Ibex Chronozone (Fig. 8). In the
434 Taylori–Polymorphus chronozones, average temperature is 15.7°C, in the Brevispina
435 Subchronozone it is 16.4°C, and in the Jamesoni Subchronozone 17.2°C. Despite
436 exhibiting more variable data, this interval was also recorded in other sections of the
437 Asturian Basin (Fig. 8) by Armendáriz et al. (2012), and relatively uniform values were
438 also recorded in the Basque–Cantabrian Basin of Northern Spain (Rosales et al., 2004)
439 and in the Peniche section of the Portuguese Lusitanian Basin (Suan et al., 2008, 2010).
440 Belemnite calcite-based $\delta^{18}\text{O}$ values published by Korte and Hesselbo (2011) are quite
441 scattered, oscillating between $\sim 1\text{‰}$ and $\sim -4.5\text{‰}$ (Fig. 8).

442 4.3.3. The Early Pliensbachian Warming interval

443 Most of the Early Pliensbachian Ibex Chronozone and the base of the Late
444 Pliensbachian are dominated by a negative excursion ranging from 1 to 1.5‰ $\delta^{18}\text{O}$,
445 representing an increase in palaeotemperature, which marks a new warming interval.
446 Average values of 18.2°C with peak values of 19.7°C were reached in the Rodiles
447 section (Fig. 7). This increase in temperature partly co-occurs with the latest part of the
448 Early Pliensbachian $\delta^{13}\text{C}$ negative excursion.

449 The Early Pliensbachian Warming interval is also well marked in other sections of
450 Northern Spain (Fig. 8) such as the Asturian Basin (Armendáriz et al., 2012) and the
451 Basque–Cantabrian Basin (Rosales et al., 2004), where peak values of around 25°C
452 were reached. The increase in seawater temperature is also registered in the Southern
453 France Grand Causses Basin (van de Shootbrugge et al., 2010), where temperatures
454 averaging approximately 18°C have been calculated. This warming interval is not so
455 clearly marked in the brachiopod calcite of the Peniche section in Portugal (Suan et al.,
456 2008, 2010), but even very scattered $\delta^{18}\text{O}$ values, and a peak palaeotemperature close
457 to 30°C, were frequently reported in the Cleveland Basin (Korte and Hesselbo, 2011).
458 In the compilation made by Dera et al. (2009, 2011) and Martínez and Dera (2015),
459 $\delta^{18}\text{O}$ values are quite scattered, but this Early Pliensbachian Warming interval is also
460 well marked. Data on neodymium isotope presented by Dera et al. (2009) indicate the
461 presence of a generalized southward current in the Euro-boreal waters for most of the
462 Early Jurassic, except for the Early–Late Pliensbachian transition, where a positive ε_{Nd}
463 excursion suggests a northward influx of warmer Tethyan or Panthalassan waters
464 which could contribute to the seawater warming detected in the Early Pliensbachian.

465 4.3.4. The Late Pliensbachian Cooling interval

466 One of the most important Jurassic $\delta^{18}\text{O}$ positive excursions is recorded in belemnites
467 from the Late Pliensbachian to the Early Toarcian in all the correlated localities (Figs. 3,
468 7, 8). This represents a significant climate change towards cooler temperatures which
469 begins at the base of the Late Pliensbachian and extends up to the earliest Toarcian
470 Tenuicostatum Chronozone, representing a major cooling interval of around 4 Myrs.
471 Average palaeotemperatures of 12.7°C for this period in the Rodiles section by
472 assuming the absence of ice caps, and peak temperatures as low as 9.5°C were
473 recorded in several samples from the Gibbosus and the Apyrenum subchronozones
474 (Fig. 7).

475 This major cooling event has been recorded in many parts of the World. In Europe, the
476 onset and the end of the cooling interval **would appear** to be synchronous at the scale
477 of the ammonites subchronozone (Fig. 8). It starts in the Stokesi Subchronozone of the
478 Margaritatus Chronozone (near the onset of the **Late** Pliensbachian), and extends up to
479 the Early Toarcian Semicelatum Subchronozone of the Tenuicostatum Chronozone. In
480 addition to the Asturian Basin (Gómez et al., 2008; Gómez and Goy, 2011; **present**
481 **paper**), it has clearly been recorded in the Basque–Cantabrian Basin (Rosales et al.,
482 2004; Gómez and Goy, 2011; García Joral et al., 2011) and in the Iberian Basin of
483 Central Spain (Gómez et al., 2008; Gómez and Arias, 2010; Gómez and Goy, 2011), in
484 the Cleveland Basin of the UK (McArthur et al., 2000; Korte and Hesselbo, 2011), in the
485 Lusitanian Basin (Suan et al., 2008, 2010), in the French Grand Causses Basin (van de
486 Schootbrugge et al., 2010), and in the data compiled by Dera et al. (2009, 2011).

487 As for many of the major cooling periods recorded in the Phanerozoic, low levels of
488 atmospheric $p\text{CO}_2$, and/or variations in oceanic currents associated with the break-up
489 of Pangea could explain these changes in seawater temperatures (Dera et al., 2009;
490 2011). The presence of relatively low $p\text{CO}_2$ levels in the Late Pliensbachian atmosphere
491 is supported by the value of ~ 900 ppm obtained from Pliensbachian araucariacean leaf
492 fossils from southeastern Australia (Steinhorsdottir and Vajda, 2015). These values are
493 much higher than the Quaternary preindustrial 280 ppm CO_2 measured (i.e. Wigley et
494 al., 1996), but lower than the ~ 1000 ppm average estimated for the Early Jurassic. The
495 Pliensbachian values recorded represent the minimum values of the Jurassic and of
496 most of the Mesozoic, as documented by the GEOCARB II (Berner, 1994), and the
497 GEOCARB III (Berner and Kothavala, 2001) curves, confirmed for the Early Jurassic by
498 Steinhorsdottir and Vajda (2015). The causes of this lowering of atmospheric $p\text{CO}_2$ are
499 unknown but they might be favoured by elevated silicate weathering rates, nutrient
500 influx, high primary productivity, and organic matter burial (Suan et al., 2010; Silva and
501 Duarte, 2015).

502 The **Late** Pliensbachian appears to represent a time interval of major cooling, likely at
503 global scale. This is why many authors point to this period as one of the main
504 candidates for the development of polar ice caps in the Mesozoic (Price, 1999; Guex et
505 al., 2001; Dera et al., 2011; Suan et al., 2011; Gómez and Goy, 2011; Fraguas et al.,
506 2012). This idea is based on the presence, in the Upper Pliensbachian deposits of
507 different parts of the World, of: 1) glendonites; 2) exotic pebble to boulder-size clasts;
508 3) the presence in some localities of a hiatus in the Late Pliensbachian–earliest
509 Toarcian; 4) the results obtained in the General Circulation Models, and 5) the Late
510 Pliensbachian palaeotemperatures calculated and the assumed pole-to-equator
511 temperature gradient.

512 **4.3.4. The Early Toarcian Superwarming interval**

513 Seawater temperature started to increase in the **earliest** Toarcian. From an average
514 temperature of 12.7°C during the **Late** Pliensbachian Cooling interval, average
515 temperature rose to 15°C in the upper part of the **earliest** Toarcian Tenuicostatum
516 Chronozone (Semicelatum Subchronozone), which represents a progressive increase in
517 seawater temperature in the order of $2\text{--}3^\circ\text{C}$. Atmospheric CO_2 concentration during
518 the **Early** Toarcian seems to have doubled from ~ 1000 ppm to ~ 2000 ppm (i.e. Berner,
519 2006; Retallack, 2009; Steinhorsdottir and Vajda, 2015), causing this intense and rapid

520 warming. Comparison of the evolution of palaeotemperature with the evolution of the
521 number of taxa reveals that progressive warming first coincides with a progressive loss
522 of taxa by several groups (Gómez and Arias, 2010; Gómez and Goy, 2011; García Joral
523 et al., 2011; Fraguas et al., 2012; Baeza-Carratalá et al., 2015) marking the prominent
524 Early Toarcian extinction interval. Seawater palaeotemperature rapidly increased
525 around the Tenuicostatum–Serpentinum zonal boundary, where average values of
526 approximately 21°C were reached, with peak temperatures of 24°C (Fig. 7). This
527 intense warming, which represents a ΔT of around 8°C with respect to the average
528 temperatures of the Late Pliensbachian Cooling interval, coincides with the turnover of
529 numerous groups (Gómez and Goy, 2011) the total disappearance of the brachiopods
530 (García Joral et al., 2011; Baeza-Carratalá et al., 2015), the extinction of numerous
531 species of ostracods (Gómez and Arias, 2010), and a crisis of the nannoplankton
532 (Fraguas, 2010; Fraguas et al., 2012; Clémence et al., 2015). Temperatures remain high
533 and relatively constant during the Serpentinum and Bifrons chronozones, and the
534 platforms were repopulated by opportunistic immigrant species that thrived in the
535 warmer Mediterranean waters (Gómez and Goy, 2011).

536 5. Conclusions

537 Several relevant climatic oscillations across the Late Sinemurian, the Pliensbachian and
538 the Early Toarcian have been documented in the Asturian Basin. Correlation of these
539 climatic changes with other European records indicates that some of these might be at
540 global scale. In the Late Sinemurian, a warm interval showing an average temperature
541 of 18.5°C was recorded. The end of this warming interval coincides with the onset of a
542 $\delta^{13}\text{C}$ negative excursion that develops throughout the latest Sinemurian and part of
543 the Early Pliensbachian.

544 The Late Sinemurian Warming interval is followed by a period of temperature
545 averaging 16°C, which develops during most of the Early Pliensbachian Jamesoni
546 Chronozone as well as the base of the Ibex Chronozone. This temperature has been
547 considered as the “normal” seawater palaeotemperature, because it coincides with
548 the average temperature of the Late Sinemurian–Early Toarcian interval studied.

549 The latest part of the Early Pliensbachian is dominated by an increase in temperature,
550 marking another warming interval which extends to the base of the Late Pliensbachian,
551 where an average temperature of 18.2 °C was calculated. Within this warming interval,
552 a $\delta^{13}\text{C}$ positive peak occurs at the transition between the Early Pliensbachian Ibex and
553 the Davoei chronozones.

554 One of the most important climatic changes was recorded throughout the Late
555 Pliensbachian. An average palaeotemperature of 12.7°C for this interval in the Rodiles
556 section delineated an about 4 Myrs major Late Pliensbachian Cooling event that was
557 recorded in many parts of the World. At least in Europe, the onset and the end of this
558 cooling interval is synchronous at the scale of the ammonites subchronozone. The
559 cooling interval coincides with a $\delta^{13}\text{C}$ slightly positive excursion, interrupted by a small
560 negative $\delta^{13}\text{C}$ peak in the latest Pliensbachian Hawskerense Chronozone. This
561 prominent cooling event has been indicated as one of the main candidates for the
562 development of polar ice caps in the Jurassic.

563 Seawater temperature started to increase in the earliest Toarcian, rising to 15°C in the
564 latest Tenuicostatum Chronozone (Semicelatum Subchronozone), and seawater
565 palaeotemperature showed a considerable increase around the
566 Tenuicostatum–Serpentinum zonal boundary, reaching average values in the order of
567 21°C, with peak intervals of 24°C, which coincides with the Early Toarcian major
568 extinction event, pointing to warming as the main cause of the faunal turnover.
569

570 Acknowledgments

571 We thank three anonymous reviewers and the editor for their comments and
572 suggestions that improved the manuscript. This research work was financed by project
573 CGL2015-66604-R of the Spanish Ministerio de Economía y Competitividad, and by
574 projects GR3/14/910431, and GI 910429 of the Universidad Complutense de Madrid.
575 Thanks to the Instituto Geológico y Minero de España for allowing the use of the
576 cathodoluminescence microscope.

577

578 References

579 Al-Suwaidi, A.H., Angelozzi, G.N., Baudin, F., Damborenea, S.E., Hesselbo, S.P., Jenkyns,
580 H.C., Manceñido, M.O. and Riccardi, A.C.: First record of the Early Toarcian
581 Oceanic Anoxic Event from the Southern Hemisphere, Neuquén Basin,
582 Argentina, *J. Geol. Soc. London*, 167, 633–636, 2010.

583 Anderson, T.F. and Arthur, M.A.: Stable isotopes of oxygen and carbon and their
584 application to sedimentologic and paleoenvironmental problems, in: *Stable*
585 *isotopes in sedimentary geology*, edited by Arthur, M.A., SEPM Short Course
586 10, 1-1-1-151, 1983.

587 Anderson, T.F., Popp, B.N., Williams, A.C., Ho, L.Z. and Hudson, J.D.: The stable isotopic
588 record of fossils from the Peterborough Member, Oxford Clay Formation
589 (Jurassic), UK: palaeoenvironmental implications. *J. Geol. Soc. London*, 151,
590 125–138, 1994.

591 Armendáriz, M., Rosales, I., Bádenas, B., Aurell, M., García-Ramos, J.C. and Piñuela, L.:
592 High-resolution chemostratigraphic record from Lower Pliensbachian
593 belemnites: Palaeoclimatic perturbations, organic facies and water mass
594 Exchange (Asturian basin, northern Spain), *Palaeogeogr. Palaeocl.*, 333–334,
595 178–191, 2012.

596 Bádenas, B., Aurell, M., García-Ramos, J.C., González, B. and Piñuela, L.: Sedimentary vs.
597 Diagenetic control on rhythmic calcareous successions (Pliensbachian of Asturias,
598 Spain), *Terra Nova*, 21, 162–170, 2009.

599 Bádenas, B., Aurell, M., Armendáriz, M., Rosales, I., García-Ramos, J.C. and Piñuela, L.:
600 Sedimentary and chemostratigraphic record of climatic cycles in Lower
601 Pliensbachian marl–limestone platform successions of Asturias (North Spain),
602 *Sed. Geol.*, 281, 119–138, 2012.

603 Baeza-Carratalá, J.F., García Joral, F., Giannetti, A. and Tent-Manclús, J.E.: Evolution of
604 the last koninckinids (Athyrida, Koninckidae), a precursor signal of the early
605 Toarcian mass extinction event in the Western Tethys, *Palaeogeogr. Palaeocl.*,
606 429, 41–56, 2015.

607 Bailey, T.R., Rosenthal, Y., McArthur, J.M., van de Shootbrugge, B. and Thirlwall, M.F.:
608 Paleoceanographic changes of the Late Pliensbachian–Early Toarcian interval: a
609 possible link to the genesis of an Oceanic Anoxic event, *Earth Planet. Sc. Lett.*,
610 212, 307–320, 2003.

611 Benito, M.I. and Reolid, M.: Belemnite taphonomy (Upper Jurassic, Western Tethys)
612 part II: Fossil–diagenetic analysis including combined petrographic and
613 geochemical techniques, *Palaeogeogr. Palaeocl.*, 358–360, 89–108, 2012.

614 Berner, R.A.: GEOCARB II: A revised model of atmospheric CO₂ over Phanerozoic time.
615 *Am. J Sci.* 249, 56–41, 1994. A revised model of atmospheric CO₂ over
616 Phanerozoic time, *Am. J. Sci.*, 249, 56–41, 1994.

617 Berner, R.A.: GEOCARBSUL: a combined model for Phanerozoic atmospheric O₂ and
618 CO₂, *Geochim. Cosmochim. Ac.*, 70, 5653–5664, 2006.

619 Berner, R.A. and Kothavala, Z. GEOCARB III. A revised model of atmospheric CO₂ over
620 Phanerozoic time, *Am. J. Sci.*, 301, 182–204, 2001.

621 Bettencourt, V. and Guerra, A.: Carbon- and Oxygen-isotope composition of the
622 cuttlebone of *Sepia officinalis*: a tool for predicting ecological information, *Mar.*
623 *Biol.*, 133, 651–657, 1999.

624 Bodin, S., Mattioli, E., Fröhlich, S., Marshall, J.D., Boutib, L., Lahsini, S. and Redfern, J.:
625 Toarcian carbon isotope shifts and nutrient changes from the Northern margin
626 of Gondwana (High Atlas, Morocco, Jurassic): Palaeoenvironmental
627 implications, *Palaeogeogr. Palaeocl.*, 297, 377–390, 2010.

628 Caruthers, A.W., Smith, P.L., Gröcke, D.R.: The Pliensbachian–Toarcian (Early Jurassic)
629 extinction: A North American perspective. in: *Volcanism, Impacts and Mass*
630 *Extinctions: Causes and Effects*, edited by Keller, G. and Kerr, A.C., *Geo. Soc.*
631 *Am. Spec. Paper* 505, 225–243, 2014.

632 Chandler, M.A., Rind, D. and Ruedy, R.: Pangaean climate during the Early Jurassic:
633 GCM simulations and the sedimentary record of paleoclimate, *Geol. Soc. Am.*
634 *Bull.*, 104, 543–559, 1992.

635 Clémence, M.E.: Pattern and timing of the Early Jurassic calcareous nannofossil crisis,
636 *Palaeogeogr. Palaeocl.*, 411, 56–64, 2014.

637 Clémence, M.E., Gardin, S. and Bartolini A.: New insights in the pattern and timing of
638 the Early Jurassic calcareous nannofossil crisis, *Palaeogeogr. Palaeocl.*, 427,
639 100–108, 2015.

640 Cohen, A.S., Coe, A.L., Harding, S.M. and Schwark, L.: Osmium isotope evidence for
641 regulation of atmospheric CO₂ by continental weathering. *Geology*, 32,
642 157–160, 2004

643 Comas-Rengifo, M.J.: *El Pliensbachiense de la Cordillera Ibérica*, PhD Universidad
644 Complutense de Madrid, 1982, Col. Tes. Doct. UCM 19/85, 1–591, 1985.

645 Comas-Rengifo, M.J. and Goy, A.: Caracterización biocronoestratigráfica del
646 Sinemuriense Superior y el Pliensbachiense entre los afloramientos de Playa de
647 Vega y de Lastres (Asturias), in: *Las sucesiones margo-calcáreas marinas del*
648 *Jurásico Inferior y las series fluviales del Jurásico Superior. Acantilados de Playa*
649 *de Vega (Ribadesella)*, edited by: García-Ramos J.C. (Coord.), *V Congreso*
650 *Jurásico de España*, MUJA, 9–18, 2010.

651 Dean, W.T. Donovan, D.T. and Howarth, M.K.: The Liassic ammonite zones and
652 subzones of the north-west European Province, *Bull. br. Mus. nat. Hist. Geol.*, 4,
653 435–505, 1961.

654 Dera, G., Pucéat, E., Pellenard, P., Neige, P., Delsate, D., Joachimski, M.M., Reisberg, L.
655 and Martinez, M.: Water mass exchange and variations in seawater
656 temperature in the NW Tethys during the Early Jurassic: Evidence from
657 neodymium and oxygen isotopes of fish teeth and belemnites, *Earth. Planet. Sc.*
658 *Lett.*, 286, 198–207, 2009.

659 Dera, G., Neige, P., Dommergues, J.L., Fara, E., Lafont, R. and Pellenard, P.: High-
660 resolution dynamics of Early Jurassic marine extinctions: the case of
661 Pliensbachian–Toarcian ammonites (Cephalopoda), *J. Geol. Soc. London*, 167,
662 21–33, 2010.

663 Dera, G., Brigaud, B., Monna, F., Laffont, R., Pucéat, E., Deconinck, J.F., Pellenard, P.,
664 Joachimski, M.M. and Durlet, C.: Climatic ups and downs in a disturbed Jurassic
665 world, *Geology*, 39, 215–218, 2011.

666 Dommergues, J.-L., Meister, C. and Mouterde, R.: Pliensbachien. in: *Grupe Français*
667 *d'Études du Jurassique: Biostratigraphie du Jurassique ouest-européen et*
668 *méditerranéen. Zonations parallèles et distribution des invertébrés et*
669 *microfossiles*, edited by: Cariou, E. and Hantzpergue, P., *Bull. cent. rech. explor. Elf-*
670 *Aquitaine*, 17, 15–24. 1997.

671 Elmi, S., Rulleau, L., Gabilly, J. and Mouterde, R.: Toarcien. *Bioestratigraphie Jurassique*
672 *ouest-européen méditerranéen: zonations parallèles et distribution des*
673 *invertébrés et microfossils*, edited by Cariou, E. and Hantzpergue, P., *Bull.*
674 *Centre Rech. Elf Explor. Prod.*, Pau, 17, 25–36, 1997.

675 Fraguas, A.: Late Sinemurian–Early Toarcian calcareous nannofossils from the
676 Cantabrian Basin: spatial and temporal distribution, PhD thesis, Fac. Sci. Geol.
677 Univ. Complutense Madrid, Spain, 2010.

678 Fraguas, A., Comas-Rengifo, M.J., Gómez, J.J. and Goy, A.: The calcareous nannofossil
679 crisis in Northern Spain (Asturias province) linked to the Early Toarcian
680 warming-driven mass extinction, *Mar. Micropaleontol.*, 94–95, 58–71, 2012.

681 Frakes, L.A., Francis, J.E. and Syktus, J.I.: Climate models of the Phanerozoic, Cambridge
682 University Press. Cambridge, 274 pp, 1992.

683 Francheschi, M., Dal Corso, J., Posenato, R., Roghi, Masetti, D. and Jenkyns, H.C.: Early
684 Pliensbachian (Early Jurassic) C-isotope perturbation and the diffusion of the
685 Lithiotis Fauna: Insights from the western Tethys, *Palaeogeogr. Palaeocl.*, 410,
686 255–263, 2014.

687 García Joral, F., Gómez, J.J. and Goy, A.: Mass extinction and recovery of the Early
688 Toarcian (Early Jurassic) brachiopods linked to climate change in northern and
689 central Spain, *Palaeogeogr. Palaeocl.*, 302, 367–380, 2011.

690 Gómez, J.J. and Arias, C.: Rapid warming and ostracods mass extinction at the Lower
691 Toarcian (Jurassic) of central Spain, *Mar. Micropaleontol.*, 74, 119–135, 2010.

692 Gómez, J.J. and Goy, A.: Warming-driven mass extinction in the Early Toarcian (Early
693 Jurassic) of northern Spain. Correlation with other time-equivalent European
694 sections, *Palaeogeogr. Palaeocl.*, 306, 176–195, 2011.

695 Gómez, J.J., Goy, A. and Canales, M.L.: Seawater temperature and carbon isotope
696 variations in belemnites linked to mass extinction during the Toarcian (Early
697 Jurassic) in Central and Northern Spain. Comparison with other European
698 sections, *Palaeogeogr. Palaeocl.*, 258, 28–58, 2008.

699 Goy, A., Comas-Rengifo, M.J., García-Ramos, J.C., Gómez, J.J., Herrero, C., Suárez-Vega,
700 L.C. and Ureta, M.: The Toarcian Stage in Asturias (North Spain): Ammonites
701 record, stratigraphy and correlations, *Earth Sci. Frontiers, Spec. Publ.*, 17,
702 38–39, 2010a.

703 Goy, A., Comas-Rengifo, M.J., Gómez, J.J., Herrero, C., Suárez-Vega, L.C. and Ureta, M.:
704 Biohorizontes de ammonoideos del Toarcienense en Asturias, edited by Ruiz
705 Omeñaca, J.J., Piñuelas, L. and García-Ramos J.C., Com. V Congreso Jurásico de
706 España, MUJA, 94–102, 2010b.

707 Guex, J., Morard, A., Bartolini, A. and Morettini, E.: Découverte d'une importante
708 lacune stratigraphique à la limite Domérien-Toarcien: implications paléo-
709 océnographiques, *Bull. Soc. Vaud. Sc. Nat.*, 87, 277–284, 2001.

710 Hallam, A.: Jurassic environments, Cambridge Earth Sci. Ser., Cambridge University
711 Press, Cambridge, 269 pp. 1975.

712 Hallam, A.: Jurassic climates as inferred from the sedimentary and fossil record, *Philos.
713 T. R. Soc. B*, 342, 287–296, 1993.

714 Harazim, D., van de Schootbrugge, B., Sorichter, K., Fiebig, J., Weug, A., Suan, G. and
715 Oschmann, W.: Spatial variability of watermass conditions within the European

755 Li, Q., McArthur, J.M., and Atkinson, T.C.: Lower Jurassic belemnites as indicators of
756 palaeo-temperature, *Palaeoclimatol. Palaeoecol.*, 315–316, 38–45, 2012.

757 Littler, K., Hesselbo, S.P. and Jenkyns, H.C.: A carbon-isotope perturbation at the
758 Pliensbachian–Toarcian boundary: evidence from the Lias Group, NE England,
759 *Geol. Mag.*, 147, 181–192, 2010.

760 Martinez, M. and Dera, G.: Orbital pacing of carbon fluxes by a ~9-My eccentricity cycle
761 during the Mesozoic. *P. Nat. Acad. Sci. USA*, 112, 12604–12609, 2015.

762 McArthur, J.M., Donovan, D.T., Thirlwall, M.F., Fouke, B.W. and Matthey, D.: Strontium
763 isotope profile of the early Toarcian (Jurassic) oceanic anoxic event, the
764 duration of ammonite biozones, and belemnite palaeotemperatures, *Earth.*
765 *Planet. Sc. Lett.*, 179, 269–285, 2000.

766 McArthur, J.M., Doyle, P., Leng, M.J., Reeves, K., Williams, T., García-Sánchez, R. and
767 Howarth, R.J.: Testing palaeo-environmental proxies in Jurassic belemnites:
768 Mg/Ca, Sr/Ca, Na/Ca, $\delta^{18}\text{O}$ and $\delta^{13}\text{C}$, *Palaeogeogr. Palaeoecol.*, 252, 464–480,
769 2007.

770 McElwain, J.C., Wade-Murphy, J. and Hesselbo, S.P.: Changes in carbon dioxide during
771 an oceanic anoxic event linked to intrusion into Gondwana coals. *Nature*, 435,
772 479–482, 2005.

773 Metodiev, L. and Koleva-Rekalova, E.: Stable isotope records ($\delta^{18}\text{O}$ and $\delta^{13}\text{C}$) of Lower-
774 Middle Jurassic belemnites from the Western Balkan mountains (Bulgaria):
775 Palaeoenvironmental application, *Appl. Geochem.*, 23, 2845–2856, 2008.

776 Mitchel, S.F.: Eight belemnite biohorizons in the Cenomanian of northwest Europe
777 and their importance. *Geol. J.*, 40, 363–382, 2005.

778 Morettini, E., Santantonio, M.; Bartolini, A., Cecca, F., Baumgartner, P.O. and Hunziker,
779 J.C.: Carbon isotope stratigraphy and carbonate production during the
780 Early–Middle Jurassic: examples from the Umbria–Marche–Sabina Apennines
781 (central Italy). *Palaeogeogr. Palaeoecol.*, 184, 251–273, 2002.

782 Mutterlose, J., Malkoc, M., Schouten, S., Sinninghe Damsté, J.S. and Foster, A.: TEX_{86}
783 and stable $\delta^{18}\text{O}$ paleothermometry of early Cretaceous sediments: Implications
784 for belemnite ecology and palaeotemperature proxy application. *Earth Planet.*
785 *Sc. Lett.*, 298, 286–298, 2010.

786 Nikitenko, B.L.: The Early Jurassic to Aalenian paleobiogeography of the arctic realm:
787 Implication of microbenthos (foraminifers and ostracodes), *Stratigr. Geol.*
788 *Correl.*, 16, 59–80, 2008.

789 Ogg, J.G. and Hinnov, L.A.: The Geologic Time Scale 2012. Chapter 26, Jurassic.
790 731–791, 2012.

791 Osete, M.L., Gómez, J.J., Pavón-Carrasco, F.J., Villalaín, J.J., Palencia, A., Ruiz-Martínez,
792 V.C. and Heller, F.: The evolution of Iberia during the Jurassic from
793 palaeomagnetic data, *Tectonophysics*, 50, 105–120, 2010.

794 Page, K.N.: The Lower Jurassic of Europe: its subdivision and correlation, Geol. Survey
795 Denmark and Greenland Bull., 1, 23–59, 2003.

796 Payne, J.L. and Kump, L.R.: Evidence for recurrent Early Triassic massive volcanism
797 from quantitative interpretation of carbon isotope fluctuations, Earth Planet.
798 Sc. Lett., 256, 264–277, 2007.

799 Phelps, M.C.: A refined ammonite biostratigraphy for the Middle and Upper Carixian (Ibex and
800 Davoei zones, Lower Jurassic) in North-West Europe and stratigraphical details of the
801 Carixian-Domerian boundary, Geobios, 18, 321–362, 1985.

802 Price, G.D.: The evidence of polar ice during the Mesozoic, Earth Sci. Rev., 48, 183–210,
803 1999.

804 Price, G. D., Twitchett, R.J., Smale, C. and Marks, V.: Isotopic analysis of the life history
805 of the enigmatic squid *Spirula spirula*, with implications for studies of fossil
806 cephalopods, Palaios, 24, 273–279, 2009.

807 Prokoph, A., Shields, G.A. and Veizer, J.: Compilation and time-series analysis of a
808 marine carbonate $\delta^{18}\text{O}$, $\delta^{13}\text{C}$, $^{87}\text{Sr}/^{86}\text{Sr}$ and $\delta^{34}\text{S}$ database through Earth history.
809 Earth Sci. Rev. 87(3), 113–133, 2013.

810 Quesada, S., Robles, S. and Rosales, I.: Depositional architecture and transgressive–
811 regressive cycles within Liassic backstepping carbonate ramps in the Basque–
812 Cantabrian Basin, northern Spain, J. Geol. Soc. London, 162, 531–548, 2005.

813 Rees, P.A., Zeigler, A.M. and Valdes, P.J.: Jurassic phytogeography and climates: new
814 data and model comparisons, in: Warm climates in Earth History, edited by
815 Huber, B., Macleod, K., Wing, S., Cambridge University Press, Cambridge, 297–
816 318, 1999.

817 Retallack, G.J.: Greenhouse crises of the past 300 million years, Geol. Soc. Am. Bull.,
818 121, 1441–1455, 2009.

819 Rexfort, A. and Mutterlose, J.: The role of biogeography and ecology on the isotope
820 signature of cuttlefishes (Cephalopoda, Sepiidae) and the impact on belemnite
821 studies, Palaeogeogr. Palaeocl., 244, 212–221, 2009.

822 Röhl, H.J., Schmid-Röhl, A., Oschmann, W., Frimmel, A. and Schwark, L.: The Posidonia
823 Shale (Lower Toarcian) of SW-Germany: an oxygen-depleted ecosystem
824 controlled by sea level and palaeoclimate, Palaeogeogr. Palaeocl., 165, 27–52,
825 2001.

826 Rosales, I., Quesada, S. and Robles, S.: Primary and diagenetic isotopic signal in fossils
827 and hemipelagic carbonates: the lower Jurassic of northern Spain,
828 Sedimentology, 48, 1149–1169, 2001.

829 Rosales, I., Quesada, S. and Robles, S.: Paleotemperature variations of Early Jurassic
830 seawater recorded in geochemical trends of belemnites from the
831 Basque–Cantabrian basin, northern Spain, Palaeogeogr. Palaeocl., 203,
832 253–275, 2004.

833 Sælen, G., Doyle, P. and Talbot, M.R.: Stable-Isotope Analyses of Belemnite Rostra
834 from the Whitby Mudstone Fm., England: Surface Water Conditions during
835 Deposition of a Marine Black Shale, *Palaios*, 11, 97–117, 1996.

836 Schmid-Röhl, A., Röhl, H.J., Oschmann, W., Frimmel, A. and Schwark, L.:
837 Palaeoenvironmental reconstruction of Lower Toarcian epicontinental black
838 shales (Posidonia Shale, SW Germany): global versus regional control, *Geobios*,
839 35, 13–20, 2002.

840 Schouten, S., van Kaam-Peters, H.M.E., Rijpstra, W.I.C., Schoell, M. and Sinninghe
841 Damste, J.S.: Effects of an oceanic anoxic event on the stable carbon isotopic
842 composition of Early Toarcian carbon, *Am. J. Sci.*, 300, 1–22, 2000.

843 Shackleton, N. J. and Kenett, J. P.: Paleotemperature history of the Cenozoic and the
844 initiation of Antarctic glaciation: Oxygen and carbon isotope analysis in DSDP
845 sites 277, 279 and 281, in: Initial Reports of the Deep Sea Drilling Projects, 29,
846 edited by: Kennet, J. P., Houtz, R. E., Andrews, P. B., Edwards, A. R., Gosting, V.
847 A., Hajós, M., Hampton, M. A., Jenkins, D.G., Margolis, S. V., Ovenshine, A. T.,
848 and Perch-Nielsen, K., US Government Printing Office, Washington, 743–756,
849 1975.

850 Silva, R.L., Duarte, L.V., Comas-Rengifo, M.J., Mendonça Filho, J.G. and Azerêdo, A.C.:
851 Update of the carbon and oxygen isotopic records of the Early–late
852 Pliensbachian (Early Jurassic, ~187Ma): insights from the organic-rich
853 hemipelagic series of the Lusitanian Basin (Portugal), *Chem. Geol.*, 283,
854 177–184. 2011.

855 Silva, R.L. and Duarte, L.V.: Organic matter production and preservation in the
856 Lusitanian Basin (Portugal) and Pliensbachian climatic snaps. *Global and Planet.*
857 *Change*, 131, 24–34. 2015.

858 Steinhorsdottir, M. and Vajda, V.: Early Jurassic (late Pliensbachian) CO₂
859 concentrations based on stomatal analysis of fossil conifer leaves from eastern
860 Australia, *Gondwana Res.*, 27, 829–897, 2015.

861 Suan, G., Mattioli, E., Pittet, B., Maillot, S. and Lécuyer, C.: Evidence for major
862 environmental perturbation prior to and during the Toarcian (Early Jurassic)
863 Oceanic Anoxic Event from the Lusitanian Basin, Portugal, *Paleoceanography*
864 23, 1202, doi: 10.1029/2007PA001459, 2008.

865 Suan, G., Mattioli, E., Pittet, B., Lécuyer, C., Suchéras-Marx, B., Duarte, L.V., Philippe,
866 M., Reggiani, F. and Martineau, F.: Secular environmental precursor to Early
867 Toarcian (Jurassic) extreme climate changes, *Earth Planet. Sc. Lett.*, 290,
868 448–458, 2010.

869 Suan, G., Nikitenko, B., Rogov, M.A., Baudin, F., Spangenberg, J.E., Knyazev, V.G.,
870 Glinskikh, L.A., Goryacheva, A.A., Adatte, T., Riding, J., Föllmi, K.B., Pittet,
871 B., Mattioli, E. and Lécuyer, C.: Polar record of Early Jurassic massive carbon
872 injection, *Earth Planet. Sc. Lett.*, 312, 102–113, 2011.

873 Suárez-Vega, L.C.: Estratigrafía del Jurásico en Asturias, Cuad. Geol. Ibérica, 3, 1–369,
874 1974.

875 Svensen, H., Planke, S., Chevalier, L., Malthe-Sørensen, A., Corfu, F. and Jamtveit, B.:
876 Hydrothermal venting of greenhouse gasses triggering Early Jurassic global
877 warming, *Earth Planet. Sc. Lett.*, 256, 554–566, 2007.

878 Ullmann, C.V. and Korte, C.: Diagenetic alteration in low-Mg calcite from macrofossils:
879 a review, *Geol. Q.*, 59, 3–20, 2015.

880 Ullmann, C.V., Thibault, N., Ruhl, M., Hesselbo, S.P. and Korte, C.: Effect of a Jurassic
881 oceanic anoxic event on belemnite ecology and evolution, *P. Nat. Acad. Sci.*
882 USA, 111, 10073–10076, 2014.

883 Valenzuela, M.: Estratigrafía, sedimentología y paleogeografía del Jurásico de Asturias,
884 Ph. D. Thesis, Fac. Sci. Geol. Univ. Oviedo, Spain, 1988.

885 Van Hinsbergen D.J.J., de Groot L.V., van Schaik S.J., Spakman W., Bijl P.K., Sluijs A.,
886 Langereis, C.G. and Brinkhuis, H.: A Paleolatitude Calculator for Paleoclimate
887 Studies. *PLoS ONE* 10(6): e0126946. doi:10.1371/journal.pone.0126946, 2015.

888 van de Shootbrugge, Harazim, D., Sorichter, K., Oschmann, W., Fiebig, J., Püttmann,
889 W., Peinl, M., Zanella, F., Teichert, B.M.A., Hoffmann, Stadnitskaia, J.A. and
890 Rosenthal, Y.: The enigmatic ichnofossil *Tissoa siphonalis* and widespread
891 authigenic seep carbonate formation during the Late Pliensbachian in southern
892 France, *Biogeosciences*, 7, 3123–3138, doi: 10.5194/bg-7-3123-2010, 2010.

893 Wierzbowski, H. and Joachimski, M.M.: Reconstruction of Late Bajocian–Bathonian
894 marine palaeoenvironments using carbon and oxygen isotope ratios of
895 calcareous fossils from the Polish Jura Chain (central Poland). *Palaeogeogr.*
896 *Palaeocl.*, 254, 523–540, 2007.

897 Wigley, T.M.L., Richels, R. and Edmonds, J.A.: Economic and environmental choices in
898 the stabilization of atmospheric CO₂ concentrations, *Nature*, 379, 240–243,
899 1996.

900 Woodfine, R.G., Jenkyns, H.C., Sarti, M., Baroncini, F. and Violante, C.: The response of
901 two Tethyan carbonate platforms to the early Toarcian (Jurassic) oceanic anoxic
902 event: environmental change and differential subsidence, *Sedimentology*, 55,
903 1011–1028, 2008.

904 Zakharov, V.A., Shurygin, B.N., Il'ina, V.I. and Nikitenko, B.L.: Pliensbachian–Toarcian
905 biotic turnover in North Siberia and the Artic Region, *Stratigr. Geol. Correl.*, 14,
906 399–417, 2006.

907

908

909 **FIGURE CAPTIONS**

910 Fig. 1. Location maps of the Rodiles section. (a): Sketched geological map of Iberia
911 showing the position of the Asturian Basin. (b): Outcrops of the Jurassic deposits in the
912 Asturian and the western part of the Basque–Cantabrian basins, and the position of
913 the Rodiles section. (c): Geological map of the Asturian Basin showing the distribution
914 of the different geological units and the location of the Rodiles section.

915

916 Fig 2. Sketch of the stratigraphical succession of the uppermost Triassic and the
917 Jurassic deposits of the Asturian Basin. The studied interval corresponds to the lower
918 part of the Santa Mera Member of the Rodiles Formation. Pli.=Pliensbachian, Toar.=
919 Toarcian. Aal.= Aalenian. Baj.=Bajocian.

920

921 Fig. 3. Stratigraphical succession of the Upper Sinemurian, the Pliensbachian and the
922 Lower Toarcian deposits of the Rodiles section, showing the lithological succession, the
923 ammonite taxa distribution, as well as the profiles of the $\delta^{18}\text{O}_{\text{bel}}$ and $\delta^{13}\text{C}_{\text{bel}}$ values
924 obtained from belemnite calcite. $\delta^{18}\text{O}_{\text{bel}}$ and $\delta^{13}\text{C}_{\text{bel}}$ in PDB. Chronozones
925 abbreviations: TEN: *Tenuicostatum*. Subchronozones abbreviations: RA: *Raricostatum*.
926 MC: *Macdonnelli*. AP: *Aplanatum*. BR: *Brevispina*. JA: *Jamesoni*. MA: *Masseanum*. LU:
927 *Luridum*. MU: *Maculatum*. CA: *Capricornus*. FI: *Figulinum*. ST: *Stokesi*. HA:
928 *Hawskerense*. PA: *Paltum*. SE: *Semicelatum*. EL: *Elegantulum*. FA: *Falciferum*.

929 Fig. 4. Thick sections photomicrographs of some of the belemnites sampled for stable
930 isotope analysis from the Upper Sinemurian and Pliensbachian of the Rodiles section.
931 The unaltered by diagenesis non luminescent sampling areas (SA), where the samples
932 have been collected, are indicated. A and B Sample ER 351, Late Sinemurian
933 *Raricostatum* Chronozone, *Aplanatum* Subchronozone. A: optical transmitted light
934 microscope, showing the carbonate deposit filling the alveolous (Cf), the outer rostrum
935 cavum wall (Cw) and fractures (Fr). B: cathodoluminescence microscope
936 photomicrograph, showing luminescence in the carbonate deposit filling the alveolous
937 (Cf), in the outer rostrum cavum wall (Cw) and in the fractures (Fr). SA represents the
938 unaltered sampling area. C and D: Sample ER 337, Early Pliensbachian *Jamesoni*
939 Chronozone, *Taylori-Polymorphus* Subchronozones. C: optical transmitted light
940 microscope, showing fractures (Fr). D: cathodoluminescence microscope
941 photomicrograph, showing luminescence in stylolites (St). SA is the unaltered sampling
942 area. E and F: Sample ER 589a Early Pliensbachian *Margaritatus* Chronozone,
943 *Subnodosus* Subchronozone. E: cathodoluminescence microscope, showing
944 luminescence in the apical line (Ap), fractures (Fr) and stylolites (St). This area of the
945 section was not suitable for sampling. F: another field of the same sample as H
946 showing scarce fractures (Fr) and the unaltered not luminescent sampled area (SA). G
947 and H: Sample ER 549a, Late Pliensbachian *Margaritatus* Chronozone, *Stokesi*
948 Subchronozone. G: cathodoluminescence microscope showing luminescent growth
949 rings (Gr) and stylolites (St). Area not suitable for sampling. H: cathodoluminescence
950 microscope photomicrograph, of the same sample as G, showing luminescent growth
951 rings (Gr) and fractures (Fr), with unaltered sampling area (SA). I: Sample ER 555 Late
952 Pliensbachian *Margaritatus* Chronozone, *Stokesi* Subchronozone.
953 Cathodoluminescence microscope photomicrograph showing luminescent growth rings

954 (Gr) and the unaltered sampling area (SA). J and K: Sample ER 623 Late Pliensbachian
955 Spinatum Chronozone, Apyrenum Subchronozone. J: cathodoluminescence
956 microscope photomicrograph showing luminescent stylolites (St). K: Another field of
957 the same sample as J showing luminescence in the apical line (Ap) and fractures (Fr) as
958 well as the non luminescent unaltered sampling area (SA). L: Sample ER 597, Late
959 Pliensbachian Margaritatus Chronozone, Gibbosus Subchronozone.
960 Cathodoluminescence microscope photomicrograph showing luminescent carbonate
961 deposit filling the alveolous (Cf), the outer and inner rostrum cavum wall (Cw), the
962 fractures (Fr) and the non luminescent sampling area (SA). Scale in bar for all the
963 photomicrographs: 1mm.

964

965 Fig. 5. Cross-plot of the $\delta^{18}\text{O}_{\text{bel}}$ against the $\delta^{13}\text{C}_{\text{bel}}$ values obtained in the Rodiles section
966 showing a cluster type of distribution. All the assayed values are within the rank of
967 normal marine values, and the correlation coefficient between both stable isotope
968 values is negative, supporting the lack of diagenetic overprints in the sampled
969 belemnite calcite. $\delta^{18}\text{O}_{\text{bel}}$ and $\delta^{13}\text{C}_{\text{bel}}$ in PDB.

970

971 Fig. 6. Correlation chart of the belemnite calcite-based $\delta^{13}\text{C}$ sketched curves across
972 Western Europe. The earliest isotopic event is the **Late** Sinemurian $\delta^{13}\text{C}$ positive
973 excursion, followed by the **Early** Pliensbachian negative excursion and the Ibex–Davoei
974 positive peak. The **Late** Pliensbachian $\delta^{13}\text{C}$ positive excursion is bounded by a $\delta^{13}\text{C}$
975 negative peak, located around the Pliensbachian–Toarcian boundary. A significant $\delta^{13}\text{C}$
976 positive excursion is recorded in the **Early** Toarcian. $\delta^{13}\text{C}_{\text{bel}}$ values in PDB..
977 Chronozones abbreviations: TEN: Tenuicostatum. SER: Serpentinum. **Ages (Ma) after**
978 **Ogg and Hinnov (2012)**.

979

980 Fig. 7. Curve of seawater palaeotemperatres of the **Late** Sinemurian, Pliensbachian
981 and Early Toarcian, obtained from belemnite calcite in the Rodiles section of Northern
982 Spain. Two warming intervals corresponding to the **Late** Sinemurian and the **Early**
983 Pliensbachian are followed by an important cooling interval, developed at the Late
984 Pliensbachian, as well as a **(super)warming** event recorded in the Early Toarcian.
985 Chronozones abbreviations: RAR: Raricostatum. D: Davoei. TENUICOSTA.:
986 Tenuicostatum. Subchronozone abbreviations: DS: Densinodulum. RA: Raricostatum.
987 MC: Macdonelli. AP: Aplanatum. BR: Bevispina. JA: Jamesoni. VA: Valdani. LU: Luridum.
988 CA: Capricornus. FI: Figulinum. SU: Subnodosus. PA: Paltum. SE: Semicelatum. FA:
989 Falciferum.

990

991 Fig. 8. Correlation chart of the belemnite calcite-based $\delta^{18}\text{O}$ sketched curves obtained
992 in different areas of Western Europe. Several isotopic events along the **latest**
993 Sinemurian, Pliensbachian and **Early** Toarcian can be recognized. The earliest event is a
994 $\delta^{18}\text{O}$ negative excursion corresponding to the **Late** Sinemurian Warming. After an
995 interval of “normal” $\delta^{18}\text{O}$ values developed in most of the Jamesoni Chronozone and

996 the **earliest** part of the Ibex Chronozone, another $\delta^{18}\text{O}$ negative excursion was
997 developed in the Ibex, Davoei and **earliest** Margaritatus chronozone, representing the
998 **Early** Pliensbachian Warming interval. A main $\delta^{18}\text{O}$ positive excursion is recorded at the
999 **Late** Pliensbachian and the **earliest** Toarcian in all the correlated localities,
1000 representing the important **Late** Pliensbachian Cooling interval. Another prominent
1001 $\delta^{18}\text{O}$ negative shift is recorded in the Early Toarcian. Values are progressively more
1002 negative in the Tenuicostatum Chronozone and suddenly decrease around the
1003 Tenuicostatum–Serpentinum zonal boundary, delineating the **Early** Toarcian $\delta^{18}\text{O}$
1004 negative excursion which represents the **Early** Toarcian (super)Warming interval.
1005 $\delta^{18}\text{O}_{\text{bel}}$ values in PDB. **Ages (Ma) after Ogg and Hinnov (2012).**

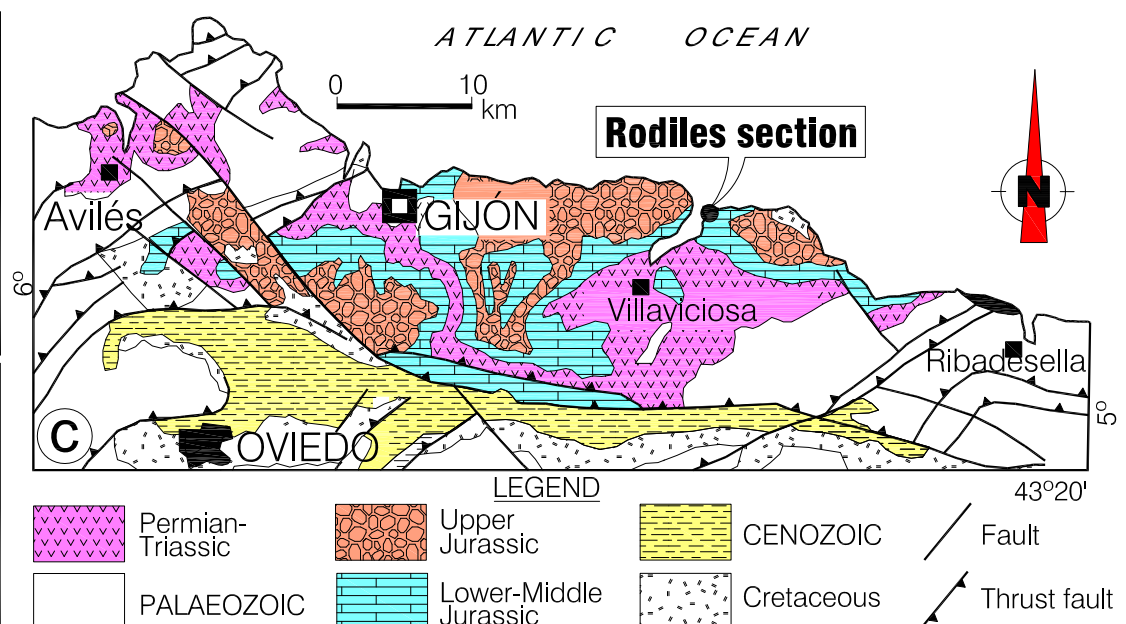
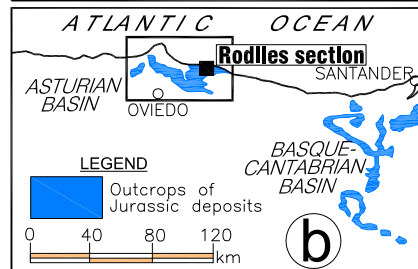
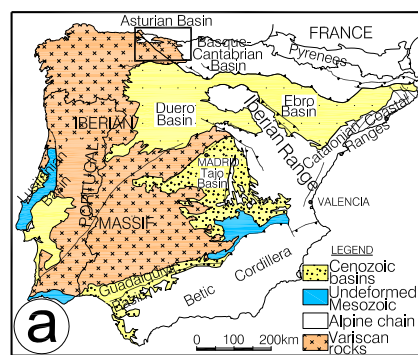


Fig. 1. Gómez, Comas-Rengifo and Goy

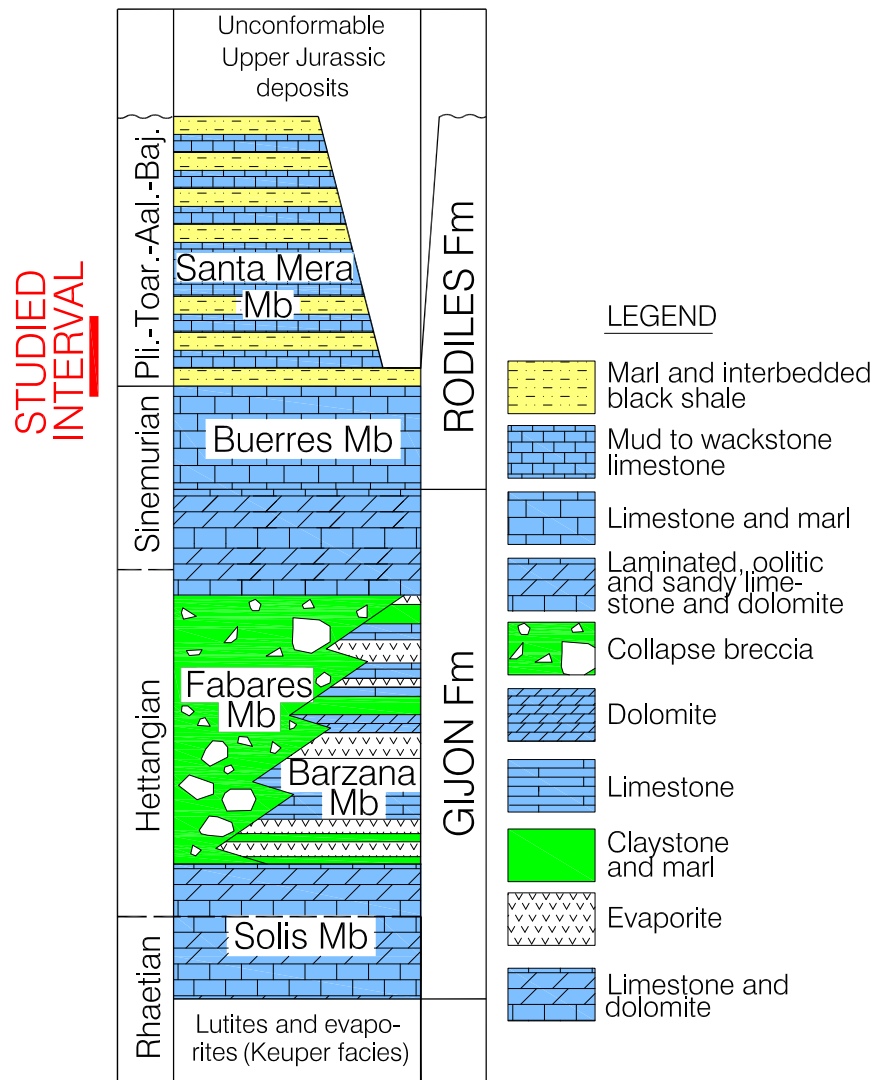


Fig. 2. Gómez, Comas-Rengifo and Goy

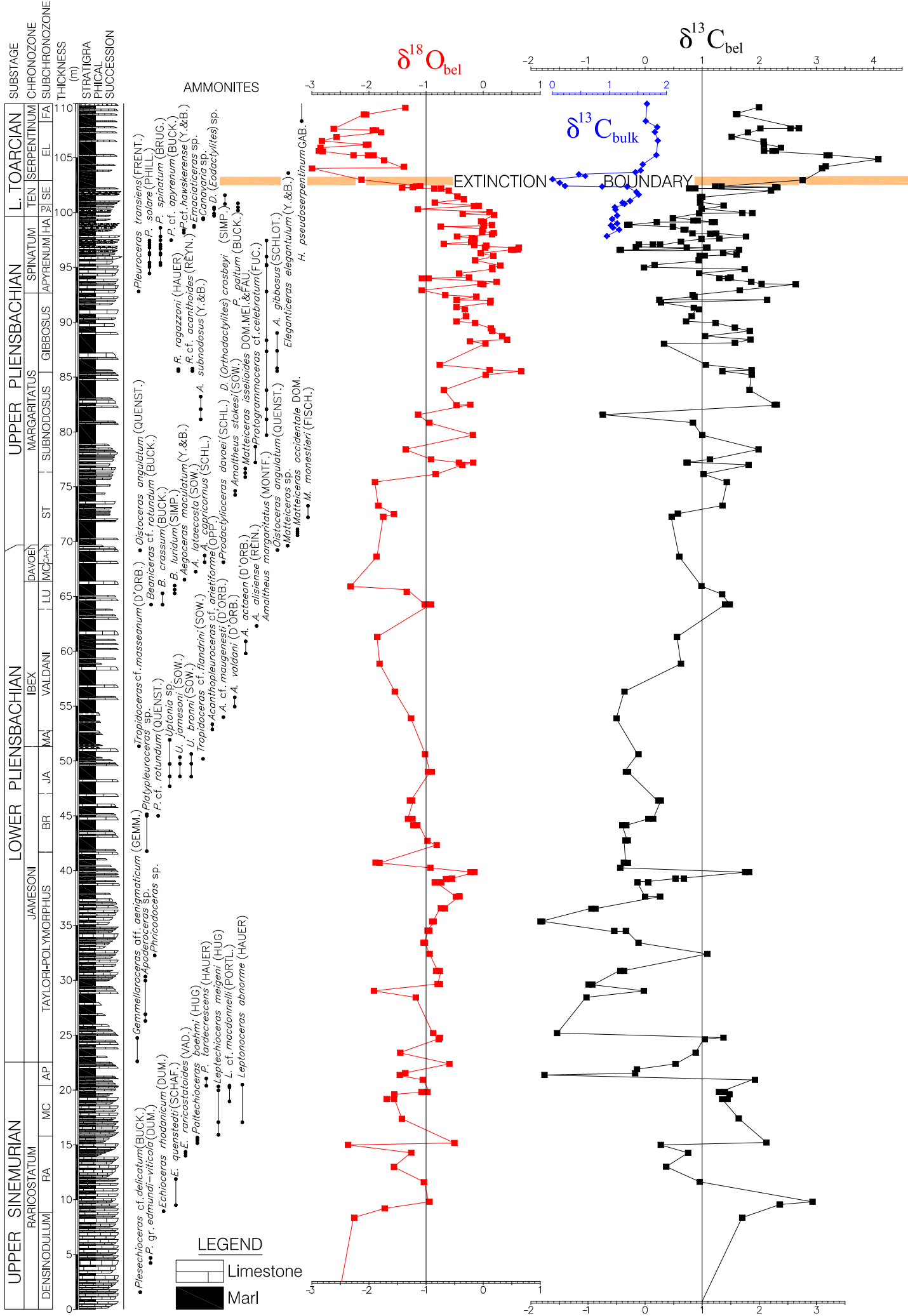


Fig. 3. Gómez, Comas-Rengifo and Goy

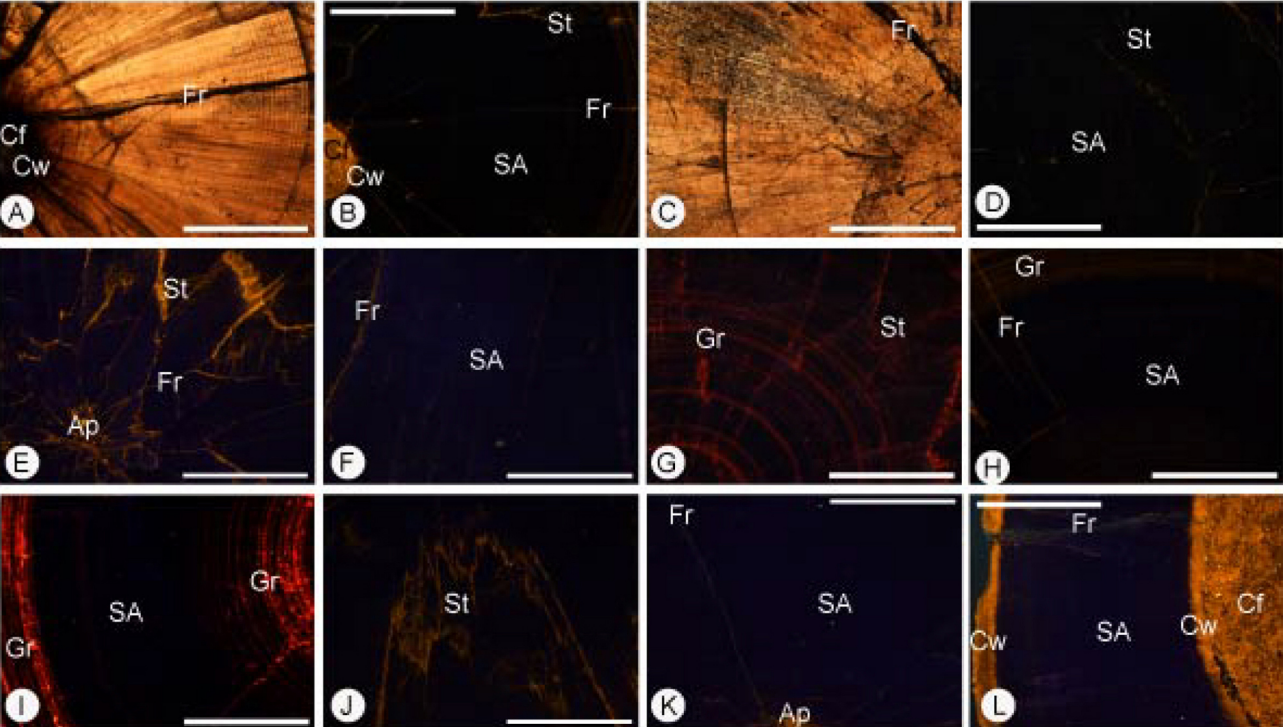


Fig 4. Gómez, Comas and Goy

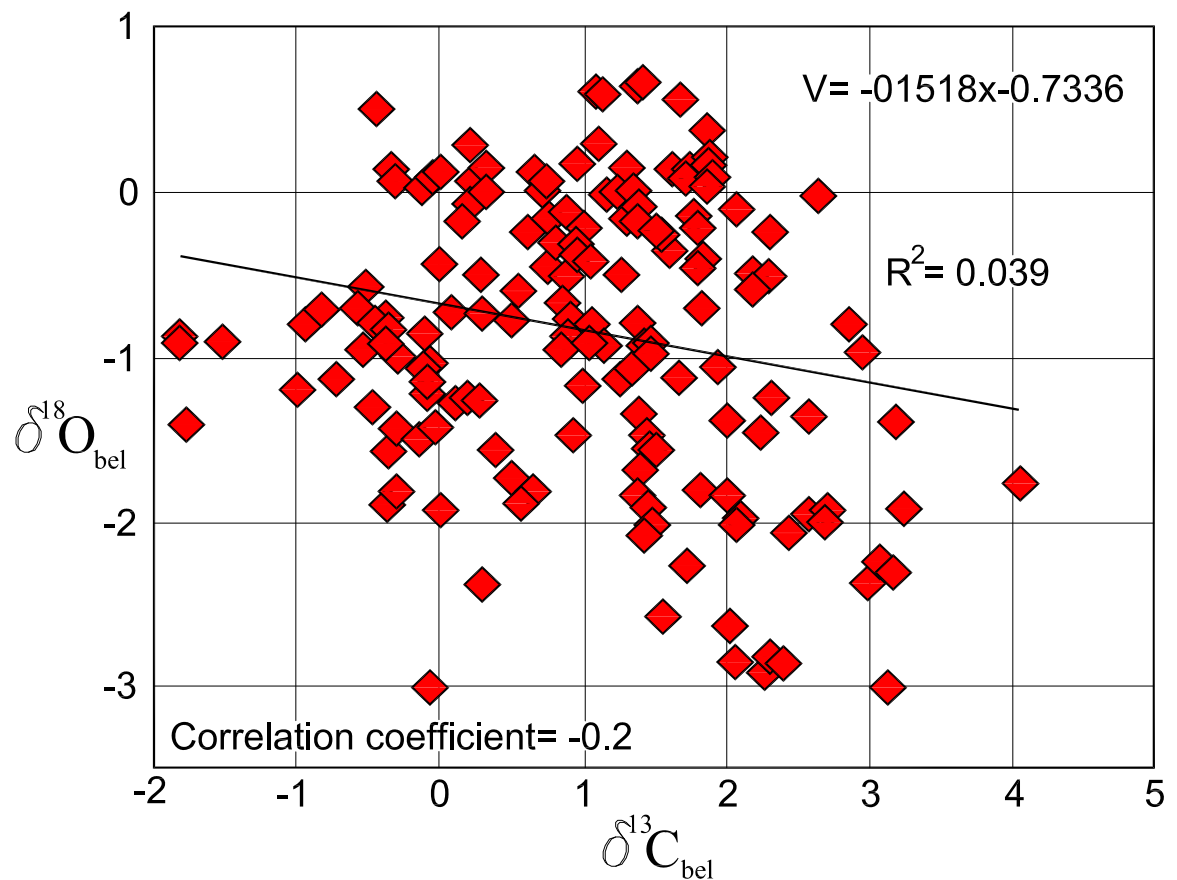
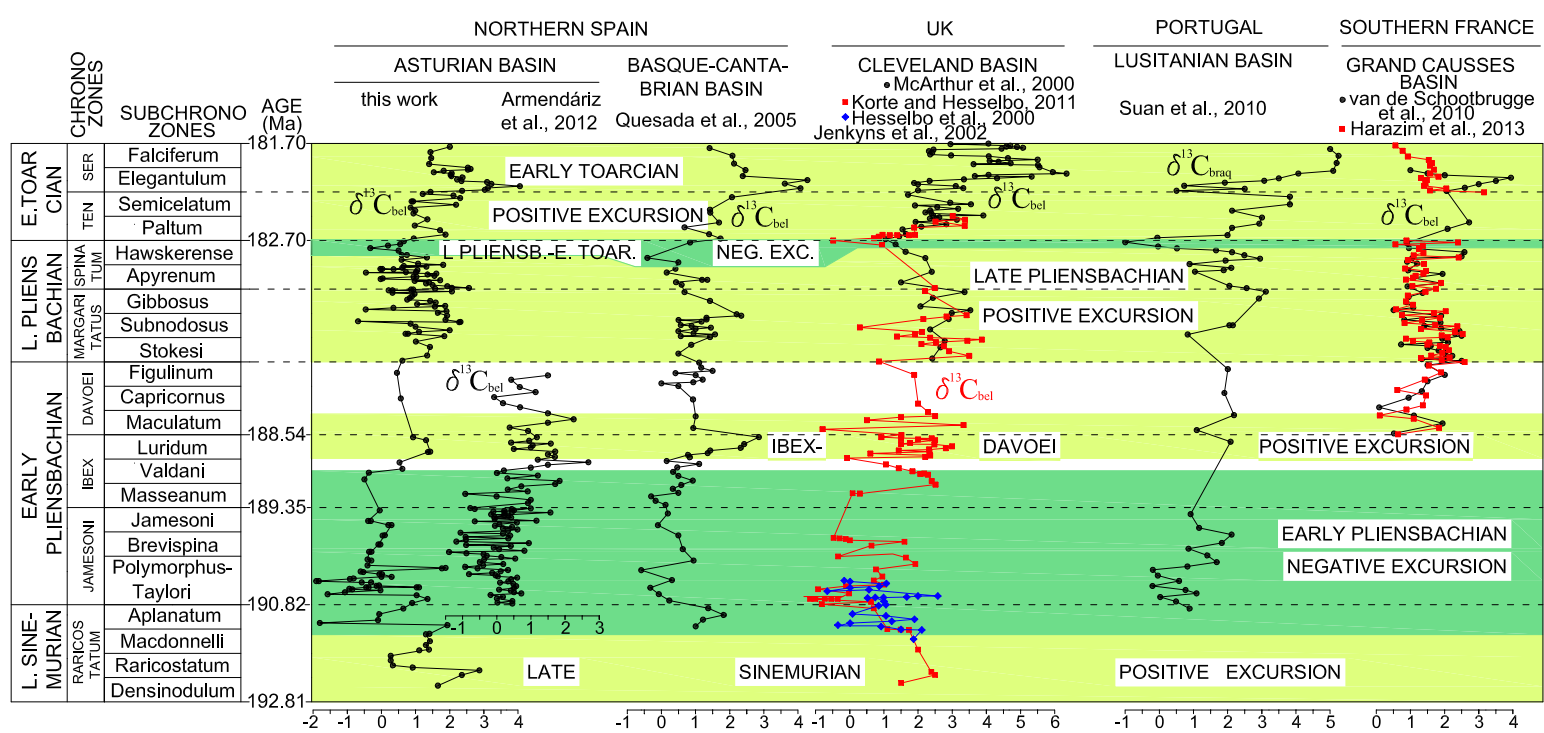


Fig. 5. Gómez, Comas-Rengifo and Goy



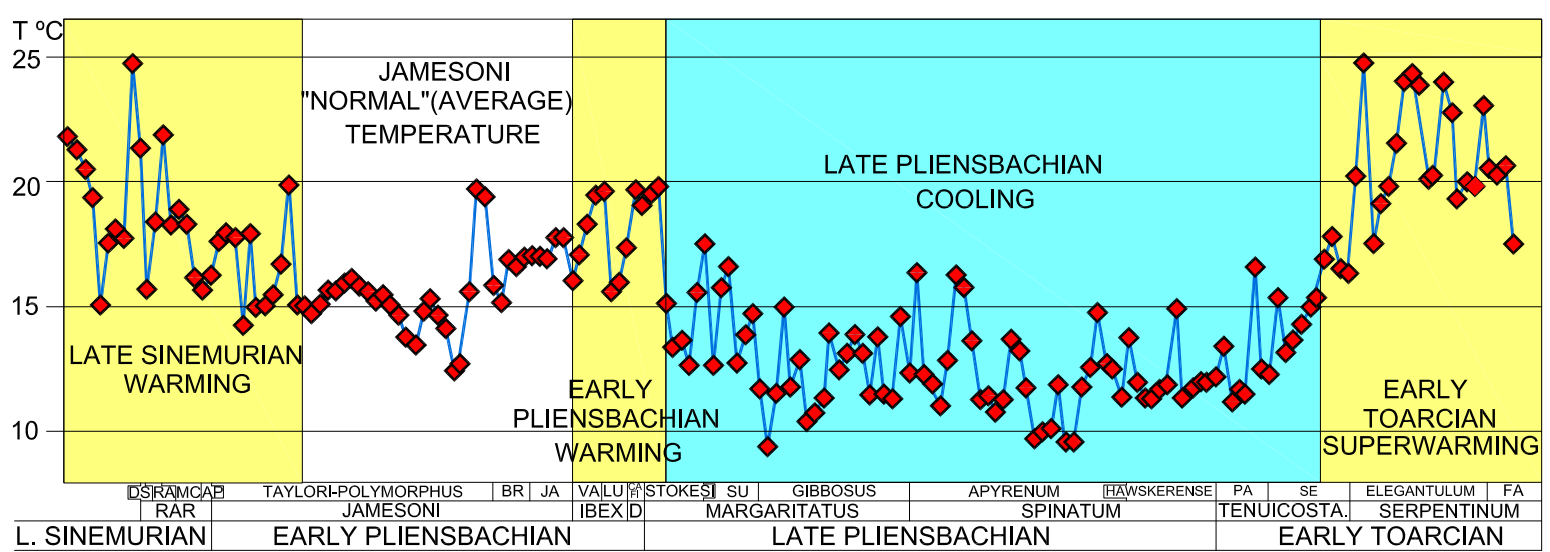


Fig. 7. Gómez, Comas-Rengifo and Goy

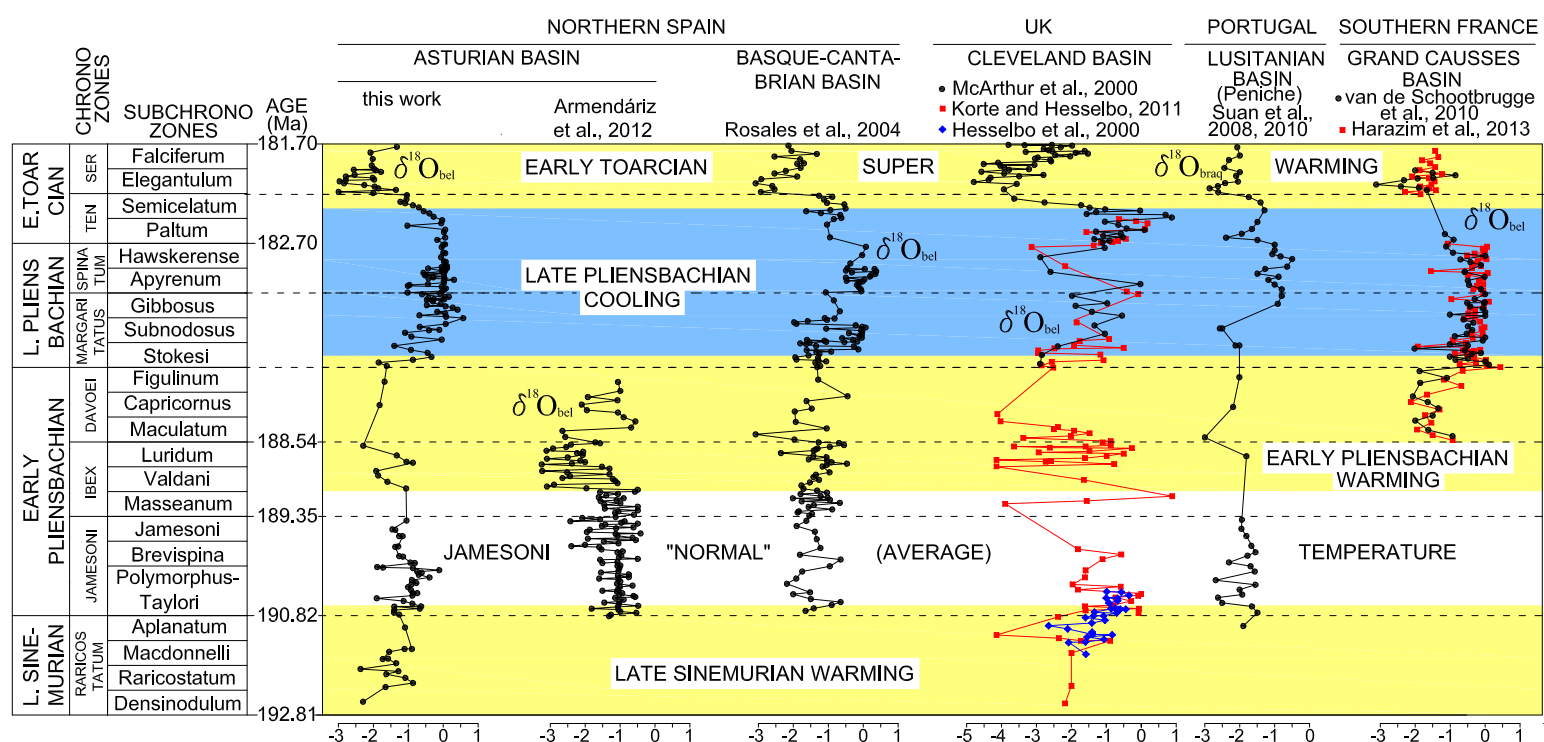


Fig. 8. Gómez, Comas-Rengifo and Goy